Supporting Information for:

In silico screening of Metal-Organic Frameworks for adsorption driven heat pumps and chillers

Máté Erdős,[†] Martijn F. de Lange,[†] Freek Kapteijn,[‡] Othonas A. Moultos,[†] and Thijs J. H. Vlugt[*,†]

†*Engineering Thermodynamics, Process & Energy Department, Faculty of Mechanical, Maritime and Materials Engineering, Delft University of Technology, Leeghwaterstraat 39, 2628CB Delft, The Netherlands*

‡*Catalysis Engineering, Chemical Engineering Department, Faculty of Applied Sciences, Julianalaan 136, 2628BL Delft, The Netherlands*

E-mail: t.j.h.vlugt@tudelft.nl

Simulation details

The Lennard-Jones parameters for the framework atoms are shown in Table S1. The force field parameters for methanol and ethanol are shown in Table S2.

Validation

The simulated and experimentally measured methanol/ethanol adsorption isotherms for the YANBAR structure at 303K and 313K are shown in Figure S1. This figure shows that the simulation and experimental results are very similar. The shapes of the isotherms are in a good agreement. It also can be observed for methanol that the experimental isotherm is shifted to lower pressures compared to the simulated isotherm.

The simulated and experimentally measured methanol and ethanol adsorption isotherms for ZIF-90 at 303K and 313K are shown in Figure S2. This figure shows that the simulation and experimental results show a reasonable agreement. The simulated loadings are higher than the experimentally measured ones. This may be caused by the fact that the defects of the structure are not taken into account in the simulations.

The simulated and experimentally measured methanol and ethanol adsorption isotherms for CuBTC (referred to as DOTSOV in DDEC[1]) at 323K are shown in Figure S3. In Figure S3 it can be seen that the experimental and simulation results differ. This behavior can be explained by the fact that the Cu-BTC structure has Coordinatively Unsaturated Sites (CUS). This means that during the adsorption process the methanol/ethanol is irreversibly adsorbed by modifying the first coordination sphere of the metal cluster.[2] Because of its irreversible nature, this phenomena is undesirable for application in AHP/ACs since it would require significantly higher desorption temperatures. The differences between the simulated and experimentally measured isotherms can be understood by considering the governing effects during the adsorption process. At the beginning of the adsorption process, methanol/ethanol molecules coordinate to the open metal sites. This effect is not accounted

for in the simulation method. The different loadings at the first part of the isotherms ($p\ p_0^{-1} < 0.04$ for methanol, $p\ p_0^{-1} < 0.03$ for ethanol, where p_0 is the experimentally measured saturation pressure of the adsorbate: $p_0 = 55.18$ kPa for methanol, $p_0 = 29.23$ kPa for ethanol)[3] is caused by the effect of the CUS. When the CUS are saturated, the clustering of the adsorbate molecules happens which results in the occurrence of the adsorption step in the isotherm. This effect is reasonable well accounted for in the simulation method as can be observed in Figure S3. The location of the adsorption step and the uptakes at the step are in a reasonable agreement for the experimental and simulated isotherms. Considering structures with larger pore dimensions, as with structures in this project, this difference caused by the CUS is less pronounced since the clustering effect becomes more dominant in determining the loadings. Hence, despite the difference at lower relative pressures the location of the adsorption step and the loadings near the step can be determined with a reasonable accuracy.

The simulated and experimentally measured methanol adsorption isotherms for the WOJJOV structure at 298K are shown in Figure S4. The synthesized structure may have defects, for example missing linkers, which is not considered during the simulations. In the simulations the reported CIF file is used which contains a perfect (without any defect) crystal structure. Therefore, the effect of the defects are not considered in the simulations which may be the cause of the observed difference in the adsorption isotherms.

The methanol adsorption isotherm of ODUNEH(Zn) structure at 293K is shown by Figure S5. It can be seen in Figure S5 that there is difference between the experimental and simulation results. In the paper which reports the synthesis of the MOF, the framework is identified as flexible.[4] Flexibility means that the MOF is capable of structural transformation towards external stimuli for instance adsorption/desorption of guest molecules.[5] Since the MOFs are considered rigid in all simulations, there is no possibility of structural transformation during the adsorption process. This lack of flexibility means that the size and shape of the pores of the simulated structure can be different from the experiments. This difference in

structural properties may be the source of the difference in the simulated and experimental isotherm. To predict the flexibility of MOFs, structure specific force field has to be derived which is very challenging and time consuming task. This prediction is computationally very expensive for a large amount of structures.

It can be concluded that the experimental isotherms are reproduced reasonably well by the simulation method and the applied force field. In case of CUS containing MOFs, it is shown that the location of the step is captured reasonably well and considering the range of diameters in the database the deviation in loadings caused by the CUS has a smaller influence. Although, the flexibility of the structures and the presence of CUS can influence the simulated results, the prediction of these properties are usually omitted in reported screening studies on MOFs.[6,7] This choice of neglecting these properties can be understood by the fact that there are no available, transferable force fields to account for the effect of CUS and neither for the flexibility for the structure.

Methanol screening

Step 2

The distribution of working capacities for the structures selected in the first step is shown in Figure S6. It can be seen that most of the structures show lower working capacity than the desired 0.4 ml working fluid per 1 ml of adsorbent.

Step 3

The new data points are computed at $p\ p_0^{-1} = 0.1$, 0.2, 0.3 and 0.4 for every structure. From the uptakes the deliverable working capacity (ΔW_{del}) is calculated. ΔW_{del} is defined as the highest difference in loading between two adjacent relative pressure points. Relative pressure intervals, where the assumed adsorption step occurs, can be defined by considering the deliverable working capacities. Based on the position of the assumed adsorption step

the structures are grouped into four bins:

- First bin: ΔW_{del} is in the range $0.05 \leq \ p\ p_0^{-1} \leq 0.1$
- Second bin: ΔW_{del} is in the range $0.1 < \ p\ p_0^{-1} \leq 0.2$
- Third bin: ΔW_{del} is in the range $0.2 < \ p\ p_0^{-1} \leq 0.3$
- Fourth bin: ΔW_{del} is in the range $0.3 < \ p\ p_0^{-1} \leq 0.4$

In Figure S7, the deliverable working capacity is shown as a function of the helium void fraction. The color coding represents the bin assigned to the structure. Isotherms for the third step are shown below per bin.

First bin:

The isotherms obtained by performing the third screening step with methanol are shown below for the structures in the first bin. The isotherms are shown in 6 figures since the large number of structures. The isotherms are shown in Figures S8-S13.

Second bin:

The isotherms obtained by performing the third screening step for methanol are shown below for the structures in the second bin. The isotherms are shown in Figures S14-S15.

Third bin:

Isotherms obtained by performing the third screening step for methanol are shown below for the structures in the third bin (Figures S16-S17).

Fourth bin:

Isotherms obtained by performing the third screening step for methanol are shown below for the structures in the fourth bin (Figure S18).

Step 4

Isotherms with the mid-density scheme:

The adsorption isotherms of each structure considered in the fourth screening step with methanol are shown in Figures S19-S42.

Ethanol screening

Step 1

In Figure S43, the calculated methanol and predicted ethanol working capacities are shown for all the structures considered in the second screening step with methanol as a function of structure density.

Step 3

The deliverable working capacity is plotted as a function of the helium void fraction for every structure is shown in Figure S44. The color code represents the bin assigned to the given structure.

Step 4

The structural properties of the structures and the results for the mid-density method with ethanol (Step 4) are shown in Table S3.

Table S1: Force field parameters (Lennard-Jones parameters) used for the framework atoms in the simulations.[8,9] The partial charges of the atoms are taken from the CIFs reported in the DDEC database.[1]

Atom	ϵ / [K]	σ / [Å]		Atom	ϵ / [K]	σ / [Å]
Ag	18.11	2.80		Mo	28.18	2.72
Al	156.00	3.91		N	38.95	3.26
As	206.34	3.70		Na	251.63	2.80
Au	19.63	2.93		Nb	29.70	2.82
B	47.81	3.58		Nd	5.03	3.19
Ba	183.19	3.30		Ne	21.14	2.89
Be	42.77	2.45		Ni	7.55	2.52
Bi	260.69	3.89		Np	9.56	3.05
Br	186.19	3.52		O	48.16	3.03
C	47.86	3.47		P	161.03	3.70
Ca	25.16	3.09		Pb	333.67	3.83
Cd	114.73	2.54		Pr	5.03	3.21
Ce	6.54	3.17		Pt	40.26	2.45
Cl	142.56	3.52		Pu	8.05	3.05
Co	7.05	2.56		Rb	20.13	3.67
Cr	7.55	2.69		Re	33.22	2.63
Cs	22.65	4.02		Rh	26.67	2.61
Cu	2.52	3.11		Ru	28.18	2.64
Dy	3.52	3.05		S	173.11	3.59
Er	3.52	3.02		Sb	225.95	3.94
F	36.48	3.09		Sc	9.56	2.94
Fe	6.54	2.59		Se	216.41	3.59
Ga	208.84	3.90		Si	156.00	3.80
Gd	4.53	3.00		Sm	4.03	3.14
Ge	201.31	3.80		Sn	276.80	3.98
H	7.65	2.85		Sr	118.27	3.24
He	10.90	2.64		Te	200.28	3.98
Hf	36.24	2.80		Th	13.09	3.03
Hg	193.76	2.41		Ti	8.55	2.83
Ho	3.52	3.04		Tm	3.02	3.01
I	256.67	3.70		U	11.07	3.03
In	301.43	3.98		V	8.05	2.80
K	17.61	3.40		W	33.72	2.73
La	8.56	3.14		Y	36.24	2.98
Li	12.58	2.18		Yb	114.75	2.99
Lu	20.63	3.24		Zn	62.40	2.46
Mg	55.86	2.69		Zr	34.72	2.78
Mn	6.54	2.64				

Table S2: Force field parameters used for methanol and ethanol in the simulations.[10]

Atom type	ϵ / [K]	σ / [Å]	q / [e]
CH_3	98	3.75	0.265
CH_2	46	3.95	0.265
O	93	3.02	-0.70
H	0.5	0.5	0.435

Bending type	Θ / [°]	k_Θ/k_B / [Krad^{-2}]
$CH_x - (O) - H$	108.5	55400
$CH_x - (CH_y) - OH$	109.5	50400

Torsion type			
$CH_x - (CH_2) - (O) - H$			
c_0/k_B / [K]	c_1/k_B / [K]	c_2/k_B / [K]	c_3/k_B / [K]
0.00	209.82	-29.17	187.93

Table S3: Summary of structural analysis of the best 12 structures with ethanol including common name, LCD, PLD, cluster type, ligands, coordination, functional groups, dimension, CUS and the references (Ref.) to the publications reporting the original MOFs.

Name	Common name	Ref.	PLD / Å	LCD / Å	Φ / -	VSA / m^2 cm^{-3}	$alpha^a$ / -	ΔW_{del}	Cluster-type	Ligand 1	Ligand 2	Coordination	Functional groups	CUS	Dim.
ANUGIA	UMCM-152	11	6.76	13.85	0.86	2137	0.04	0.558	$[Cu_2]^{4+}$	$[H_7C_14O_4]^{4-}$	-	CL(1)	-	Yes	3D
RUVKAV	PCN-46	12	7.15	11.95	0.83	2149	0.04	0.594	$[Cu_2]^{4+}$	$[H_6C_20O_8]^{4-}$	-	CL(1)	-	Yes	3D
FUNBOG	-	13	11.01	12.59	0.78	1962	0.05	0.544	$[Zn_2]^{4+}$	$[H_16C_34O_8Br_2]^{4-}$	$[H_8C_10N_4]$	CL(1)L(2)	(C)-Br	No	3D
IYIHUU	-	14	10.44	11.84	0.73	1892	0.05	0.447	$[Zn_2]^{4+}$	$[H_16C_34O_8Br_2]^{4-}$	$[H_10C_16N_2]$	CL(1)L(2)	(C)-Br	No	3D
ZECKOJ	-	15	7.76	10.01	0.74	2140	0.05	0.472	$[Cu_2]^{4+}$	$[H_6C_6O_2N_2]^{2-}$	-	C(L1)2	-	Yes	3D
FUNCEX	-	13	12.48	13.22	0.81	1873	0.07	0.294	$[Zn_2]^{4+}$	$[H_16C_34O_8Br_2]^{4-}$	$[H_8C_12N_6]$	CL(1)L(2)	(C)-Br	No	3D
IRMOF-6	IRMOF-6	16	6.71	15.04	0.77	2079	0.07	0.426	$[Zn_4O]^{6+}$	$[H_6C_10O_4]^{2-}$	-	CL(1)3	-	No	3D
XEBHOC	Cu_2(TCPPDA)	17	9.91	12.08	0.86	2170	0.07	0.646	$[Cu_2]^{4+}$	$[H_20C_34O_8N_2]^{4-}$	-	CL(1)	-	Yes	3D
FEFDEB	DMOF-1-bpdc	18	11.61	13.11	0.76	1873	0.08	0.54	$[Zn_2]^{4+}$	$[H_8C_14O_4]^{2-}$	$[H_12C_6N_2]$	CL(1)2L(2)	-	No	3D
PEVQEO	IRMOF-1	16	7.95	14.86	0.84	2184	0.08	0.638	$[Zn_4O]^{6+}$	$[H_4C_8O_4]^{2-}$	-	CL(1)3	-	No	3D
HAFTOZ	-	19	7.52	15.37	0.81	2005	0.1	0.606	$[Ni_8]^{12+}$	$[H_6C_15N_6]^{2-}$	-	CL(1)6	-	No	3D
GUNFAW01	-	20	7.34	9.61	0.74	2301	0.23	0.653	$[CrMn]^{5+}$	$[C_2O_4]^{2-}$	-	CL(1)3	-	Yes	3D

[a]- α represents the relative pressure value where the loading is equal to the half of the possible maximum loading of the structure.

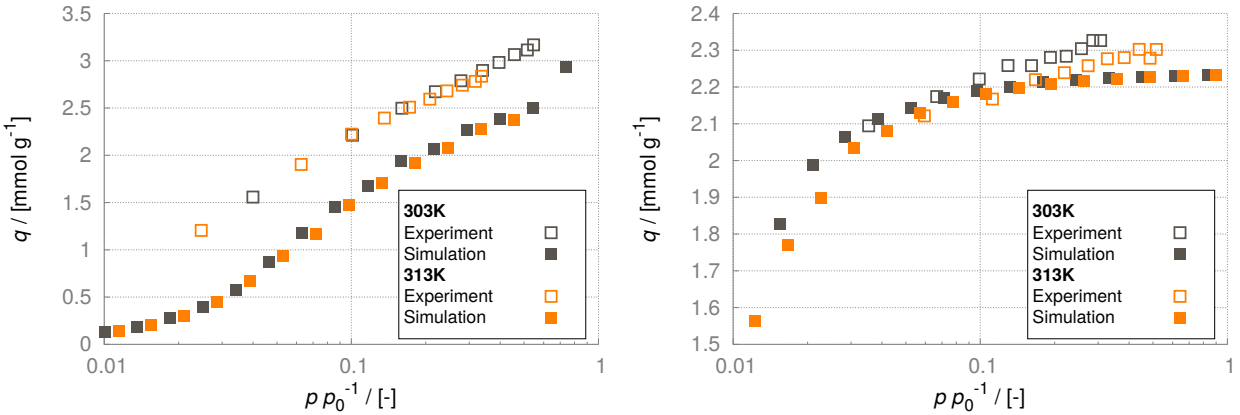

Figure S1: The excess amount of adsorbed methanol (left) and ethanol (right) as a function of relative pressure, $p\ p_0^{-1}$ (where p_0 is the saturation pressure of the adsorbate), for the YANBAR structure at 308 K (for methanol $p_0 = 27.75$ kPa, for ethanol $p_0 = 13.65$ kPa[3]) and 313 K (for methanol $p_0 = 35.18$ kPa, for ethanol $p_0 = 17.75$ kPa).[3] Experimental data is reproduced from literature.[21] The experimental and simulation results are depicted by open and closed symbols, respectively.

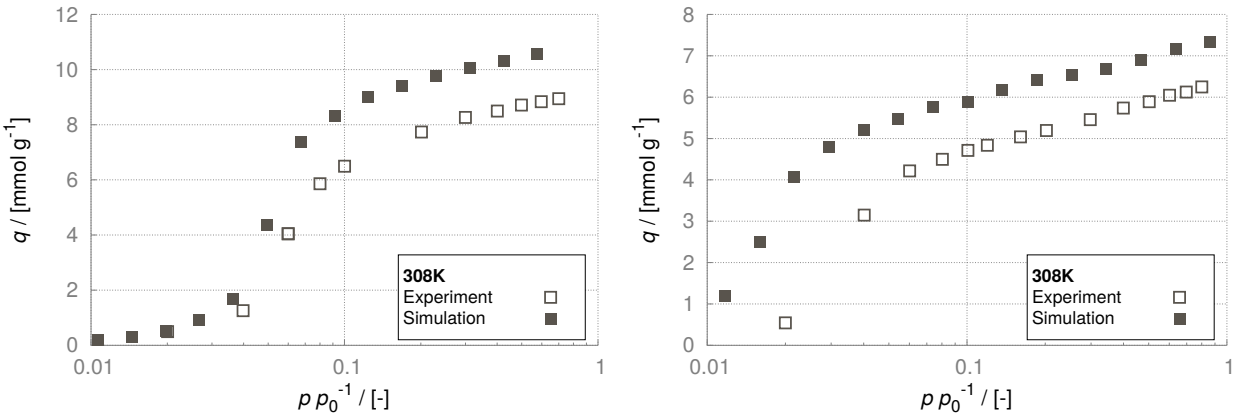

Figure S2: The excess amount of adsorbed methanol (left) and ethanol (right) as a function of relative pressure, $p\ p_0^{-1}$ (where p_0 is the saturation pressure of the adsorbate), for ZIF-90 at 308 K (for methanol $p_0 = 27.75$ kPa, for ethanol $p_0 = 13.65$ kPa).[3] Experimental data is reproduced from literature.[22] The experimental and simulation results are depicted by open and closed symbols, respectively.

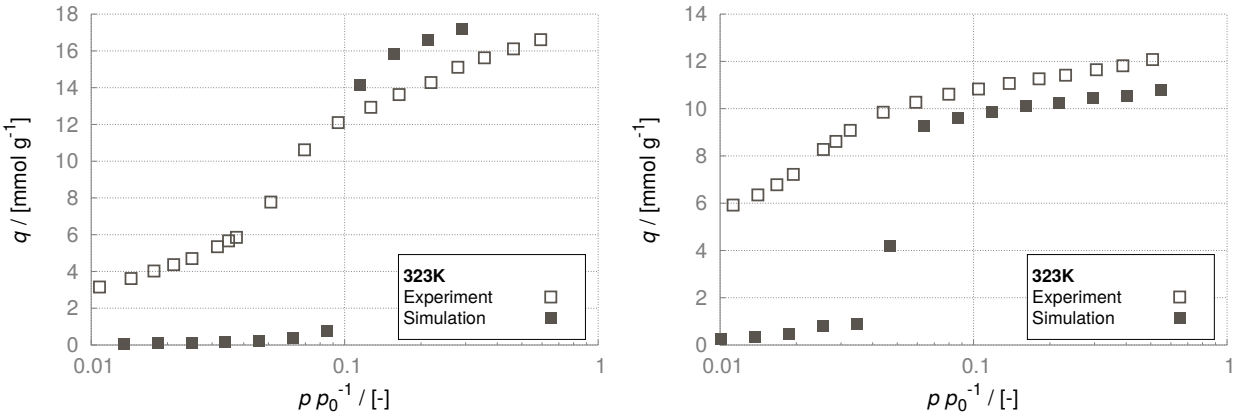

Figure S3: The excess amount of adsorbed methanol (left) and ethanol (right) as a function of relative pressure, $p\ p_0^{-1}$ (where p_0 is the saturation pressure of the adsorbate), for CuBTC at 323K (for methanol $p_0 = 55.18$ kPa, for ethanol $p_0 = 29.23$ kPa).[3] Experimental data is reproduced from literature.[23] The experimental and simulation results are depicted by open and closed symbols, respectively.

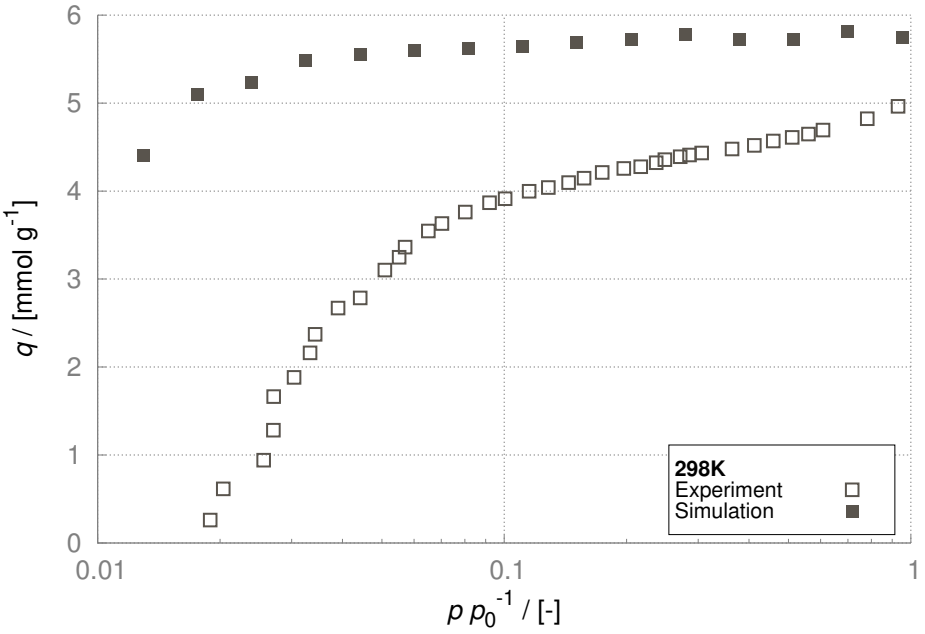

Figure S4: The excess amount of adsorbed methanol (left) and ethanol (right) as a function of relative pressure, $p\ p_0^{-1}$ (where p_0 is the saturation pressure of the adsorbate), for the WOJJOV structure at 298K (for methanol $p_0 = 16.81$ kPa, for ethanol $p_0 = 7.82$ kPa).[3] Experimental data is reproduced from literature.[4] The experimental and simulation results are depicted by open and closed symbols, respectively.

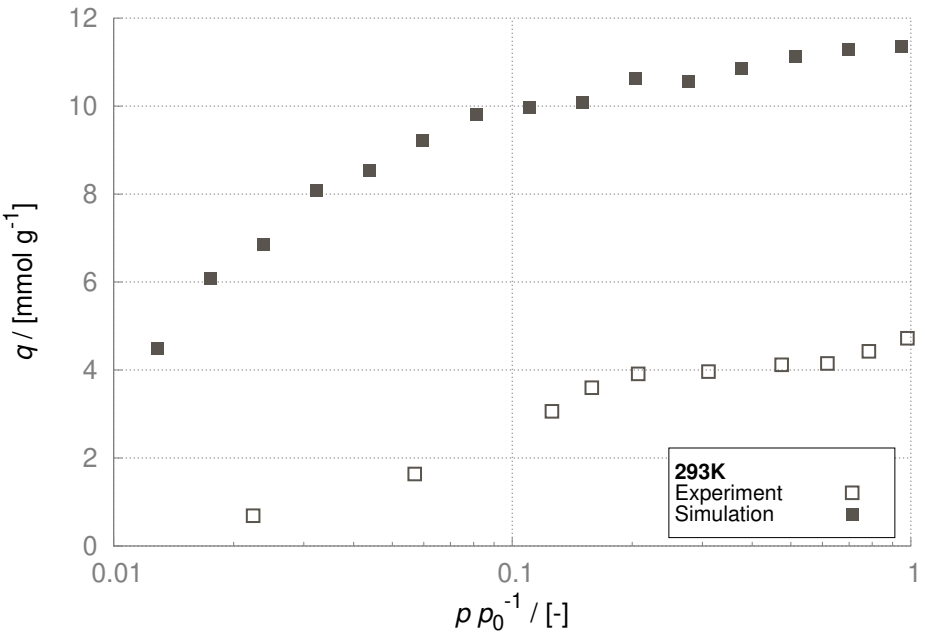

Figure S5: The excess amount of adsorbed methanol as a function of relative pressure, $p\ p_0^{-1}$ (where p_0 is the saturation pressure of the adsorbate), for the ODUNEH structure at 293K ($p_0 = 12.89$ kPa).[3] Experimental data is reproduced from literature.[24] The experimental and simulation results are depicted by open and closed symbols, respectively.

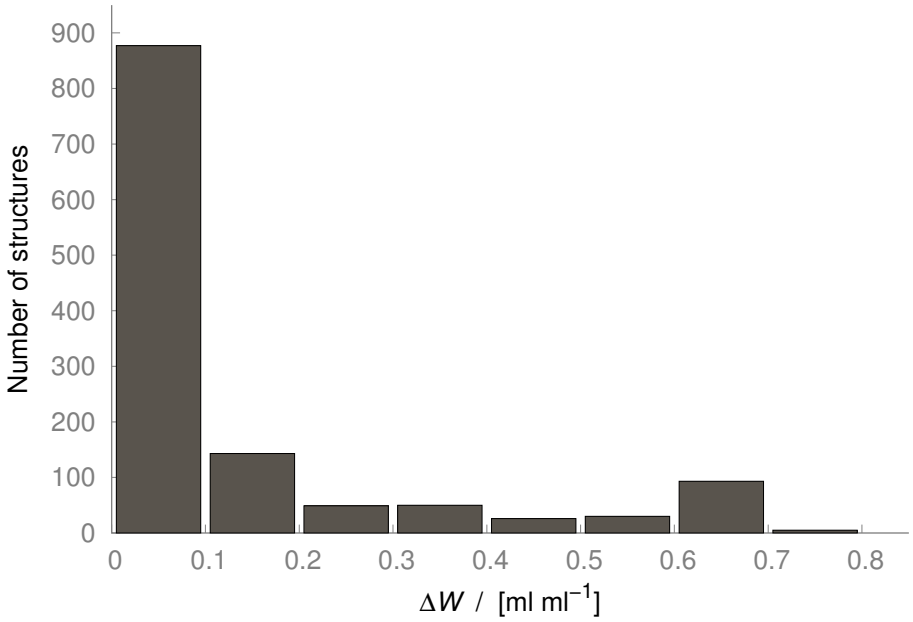

Figure S6: The number distribution of working capacities calculated for each structures considered in the second screening step with methanol.

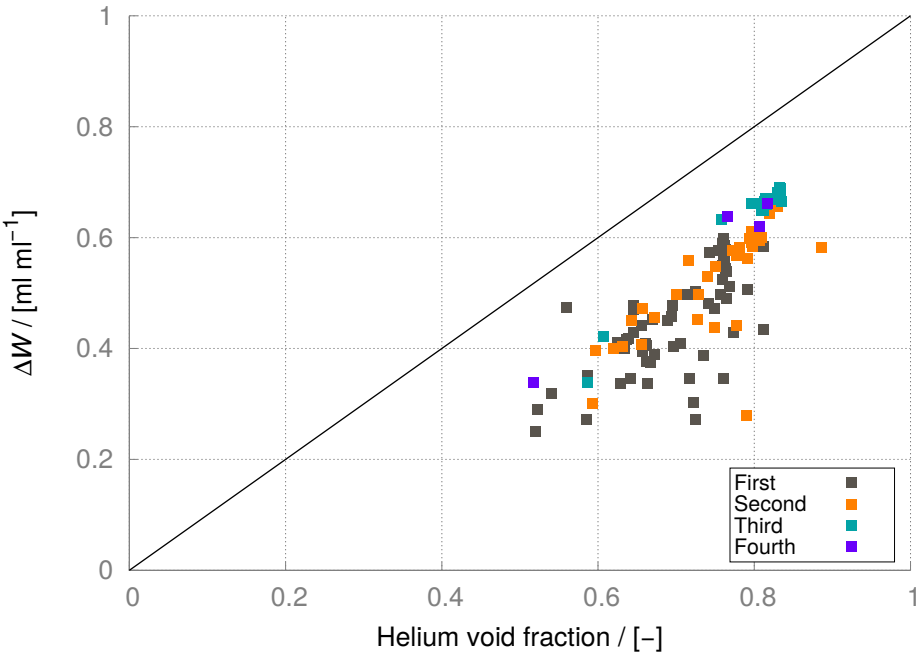

Figure S7: Deliverable working capacity shown as a function of the helium void fraction. The color code is used to indicate the interval where the assumed adsorption step for methanol occurs. The intervals are defined as follows, First: $0.05 \leq p\,p_0^{-1} \leq 0.1$, Second: $0.1 < p\,p_0^{-1} \leq 0.2$, Third: $0.2 < p\,p_0^{-1} \leq 0.3$, Fourth: $0.3 < p\,p_0^{-1} \leq 0.4$.

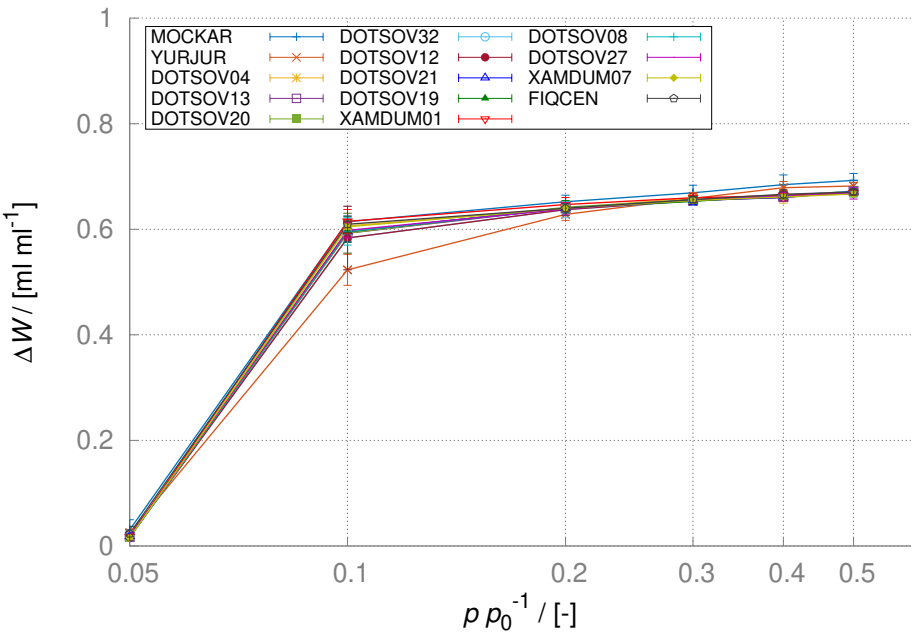

Figure S8: The excess amount of adsorbed methanol as a function of relative pressure ($p\,p_0^{-1}$, where p_0 is the saturation pressure of the adsorbate, $p_0 = 21.7$ kPa)[3] for the structures in the first bin at the third selection step. The error bars indicate the 95% confidence intervals.

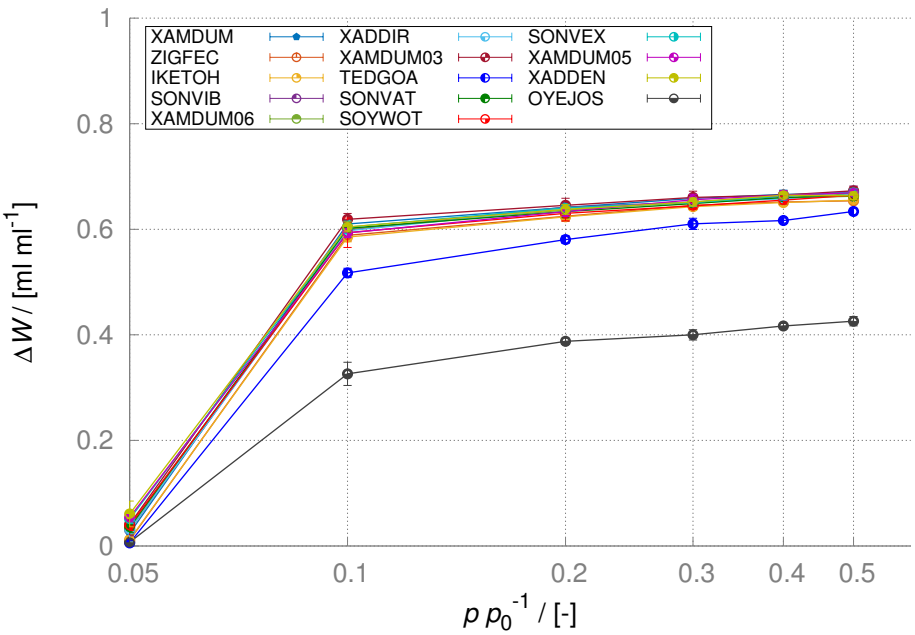

Figure S9: The excess amount of adsorbed methanol as a function of relative pressure ($p\,p_0^{-1}$, where p_0 is the saturation pressure of the adsorbate, $p_0 = 21.7$ kPa)[3] for the structures in the first bin at the third selection step. The error bars indicate the 95% confidence intervals.

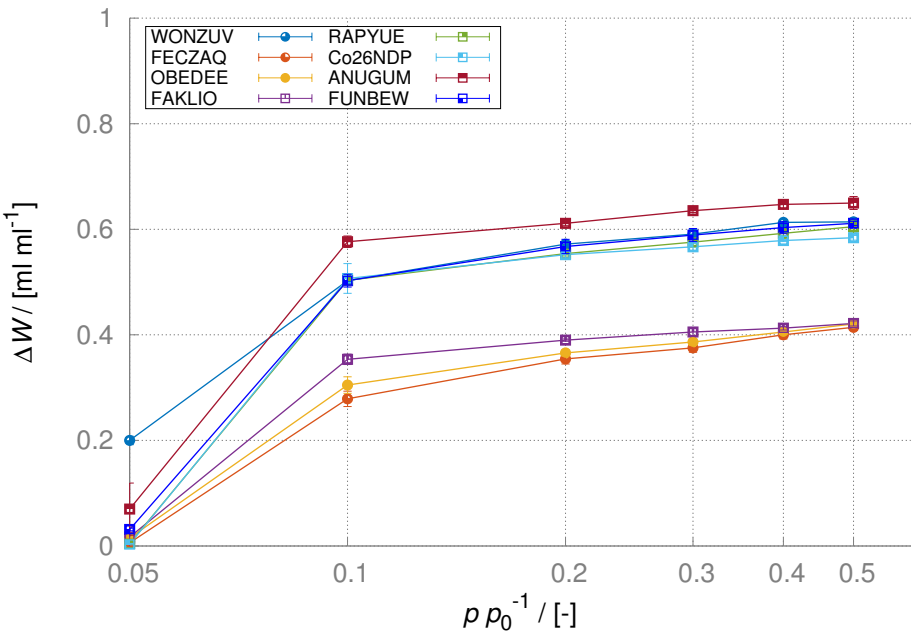

Figure S10: The excess amount of adsorbed methanol as a function of relative pressure ($p\,p_0^{-1}$, where p_0 is the saturation pressure of the adsorbate, $p_0 = 21.7$ kPa)[3] for the structures in the first bin at the third selection step. The error bars indicate the 95% confidence intervals.

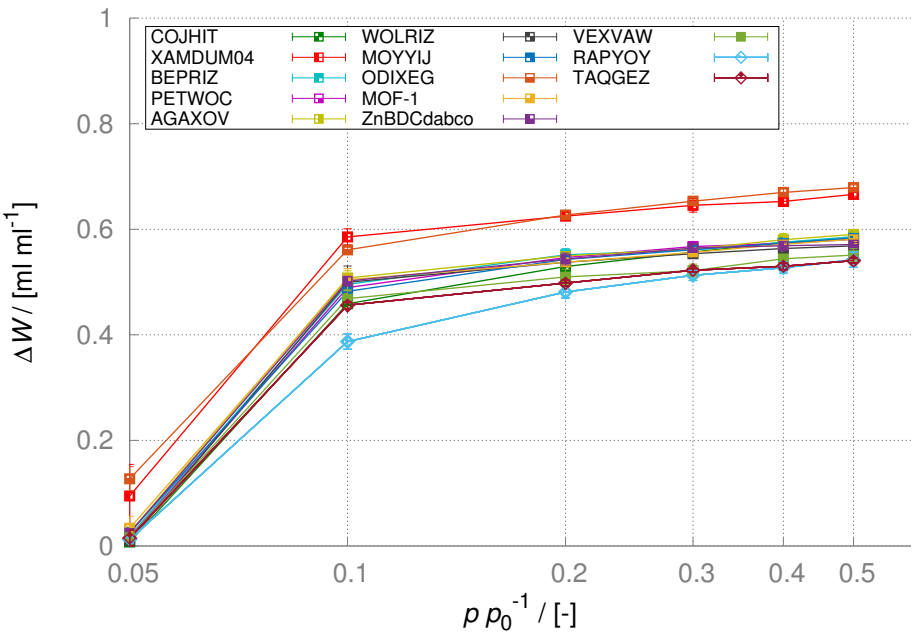

Figure S11: The excess amount of adsorbed methanol as a function of relative pressure ($p\,p_0^{-1}$, where p_0 is the saturation pressure of the adsorbate, $p_0 = 21.7$ kPa)[3] for the structures in the first bin at the third selection step. The error bars indicate the 95% confidence intervals.

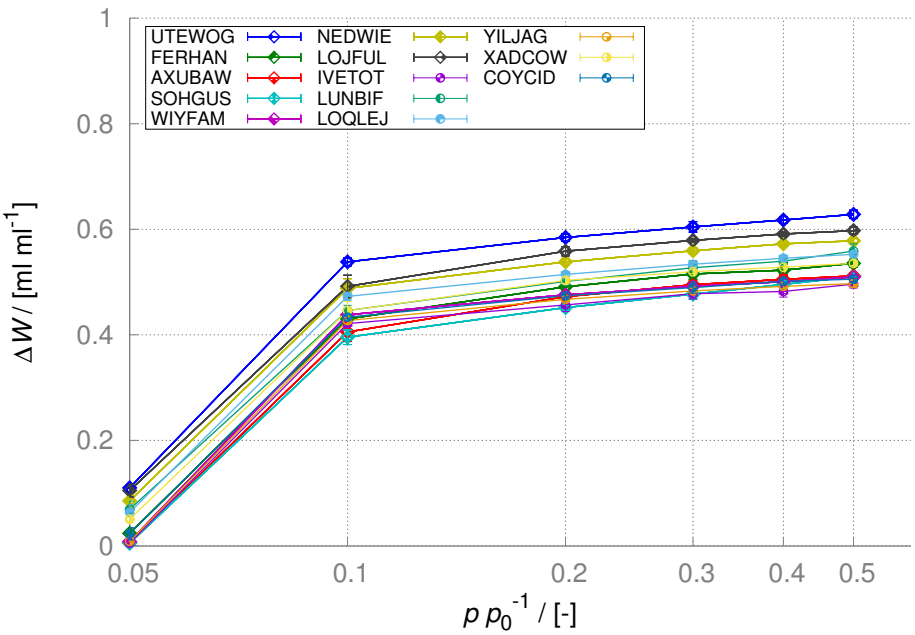

Figure S12: The excess amount of adsorbed methanol as a function of relative pressure ($p\,p_0^{-1}$, where p_0 is the saturation pressure of the adsorbate, $p_0 = 21.7$ kPa)[3] for the structures in the first bin at the third selection step. The error bars indicate the 95% confidence intervals.

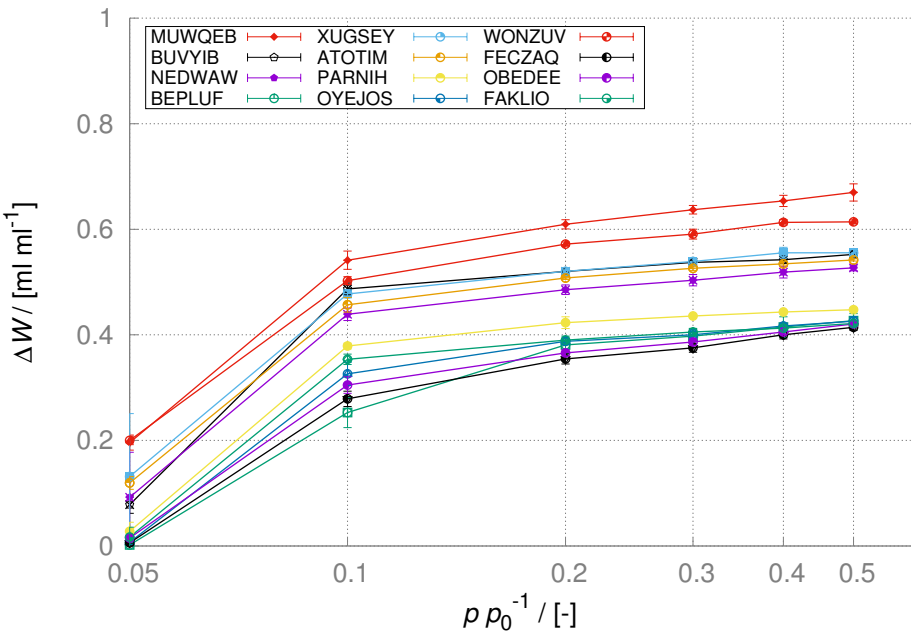

Figure S13: The excess amount of adsorbed methanol as a function of relative pressure ($p\,p_0^{-1}$, where p_0 is the saturation pressure of the adsorbate, $p_0 = 21.7$ kPa)[3] for the structures in the first bin at the third selection step. The error bars indicate the 95% confidence intervals.

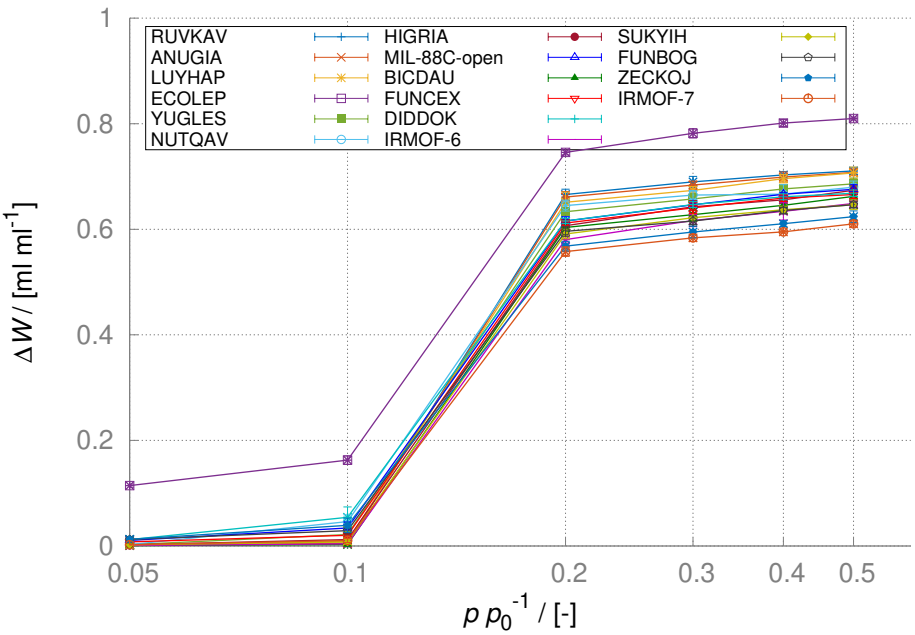

Figure S14: The excess amount of adsorbed methanol as a function of relative pressure ($p\,p_0^{-1}$, where p_0 is the saturation pressure of the adsorbate, $p_0 = 21.7$ kPa)[3] for the structures in the second bin at the third selection step. The error bars indicate the 95% confidence intervals.

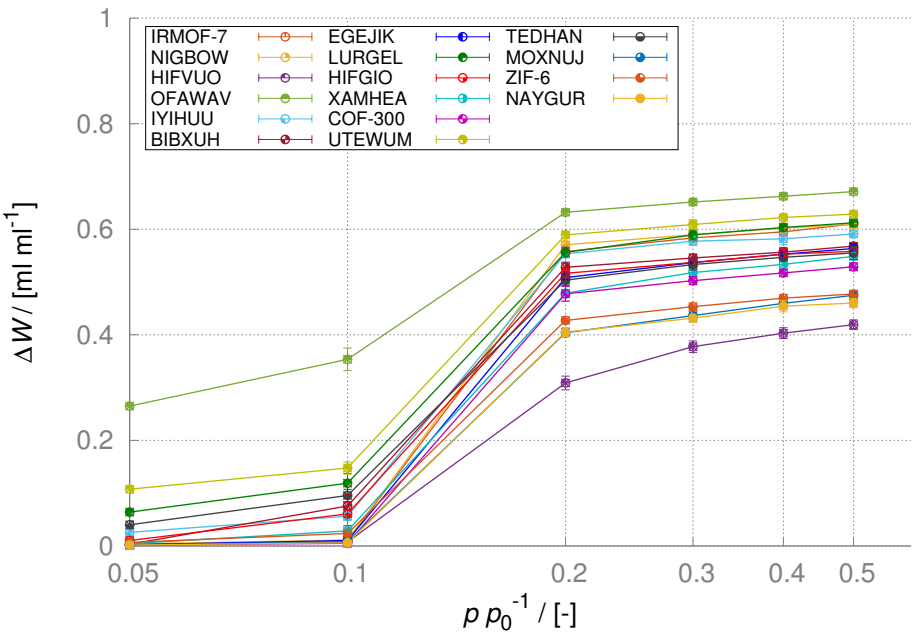

Figure S15: The excess amount of adsorbed methanol as a function of relative pressure ($p\,p_0^{-1}$, where p_0 is the saturation pressure of the adsorbate, $p_0 = 21.7$ kPa)[3] for the structures in the second bin at the third selection step. The error bars indicate the 95% confidence intervals.

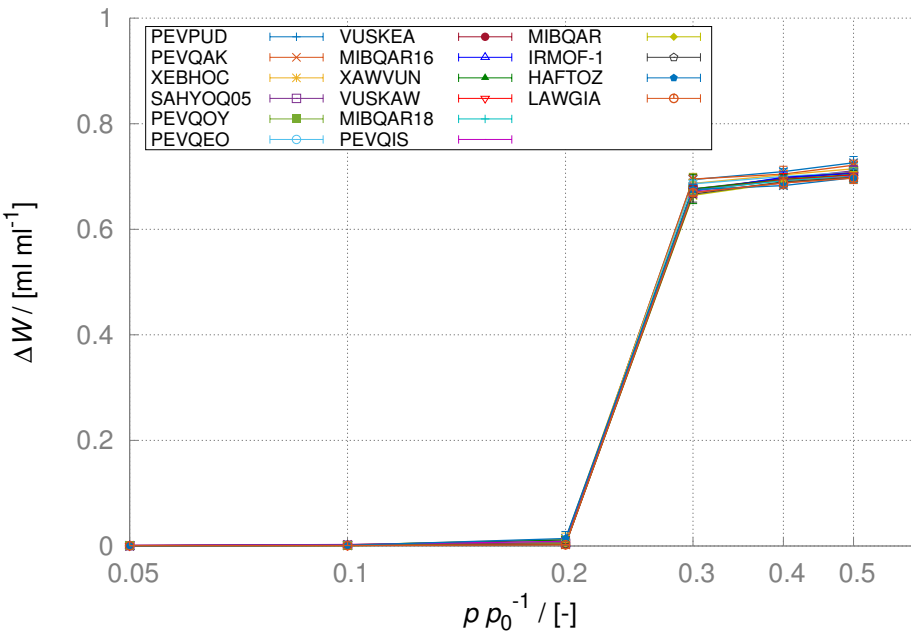

Figure S16: The excess amount of adsorbed methanol as a function of relative pressure ($p\,p_0^{-1}$, where p_0 is the saturation pressure of the adsorbate, $p_0 = 21.7$ kPa)[3] for the structures in the third bin at the third selection step. The error bars indicate the 95% confidence intervals.

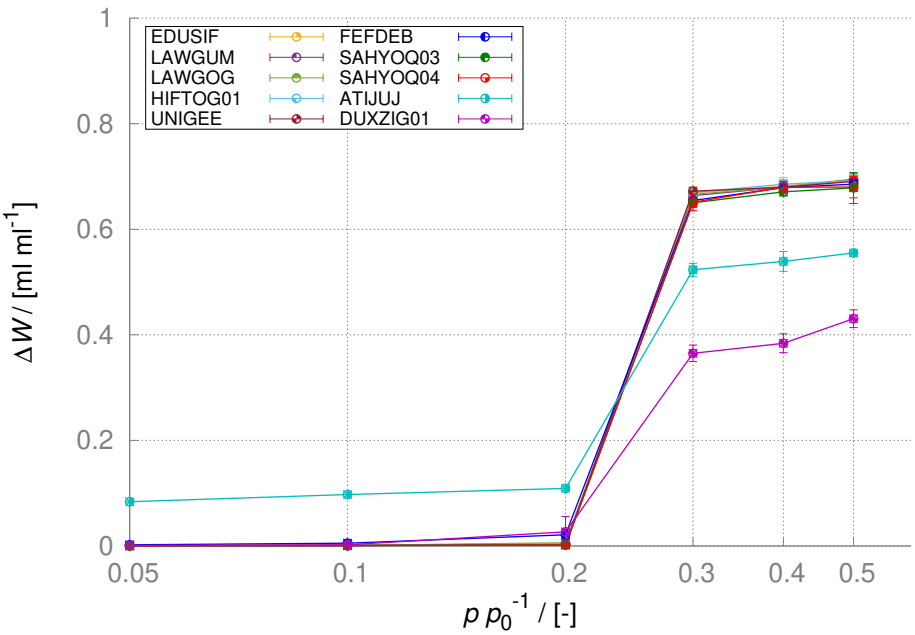

Figure S17: The excess amount of adsorbed methanol as a function of relative pressure ($p\,p_0^{-1}$, where p_0 is the saturation pressure of the adsorbate, $p_0 = 21.7$ kPa)[3] for the structures in the third bin at the third selection step. The error bars indicate the 95% confidence intervals.

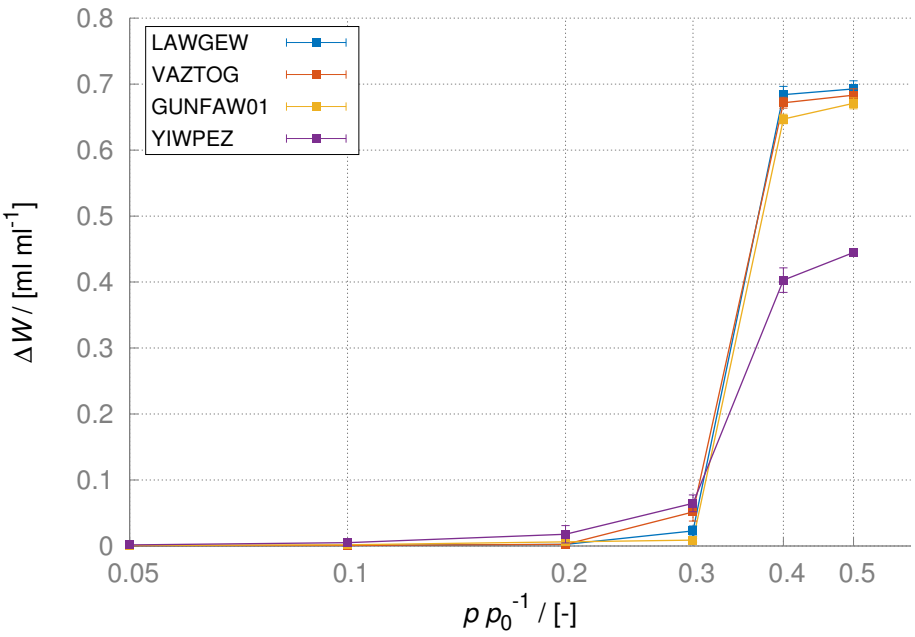

Figure S18: The excess amount of adsorbed methanol as a function of relative pressure ($p\,p_0^{-1}$, where p_0 is the saturation pressure of the adsorbate, $p_0 = 21.7$ kPa)[3] for the structures in the fourth bin at the third selection step. The error bars indicate the 95% confidence intervals.

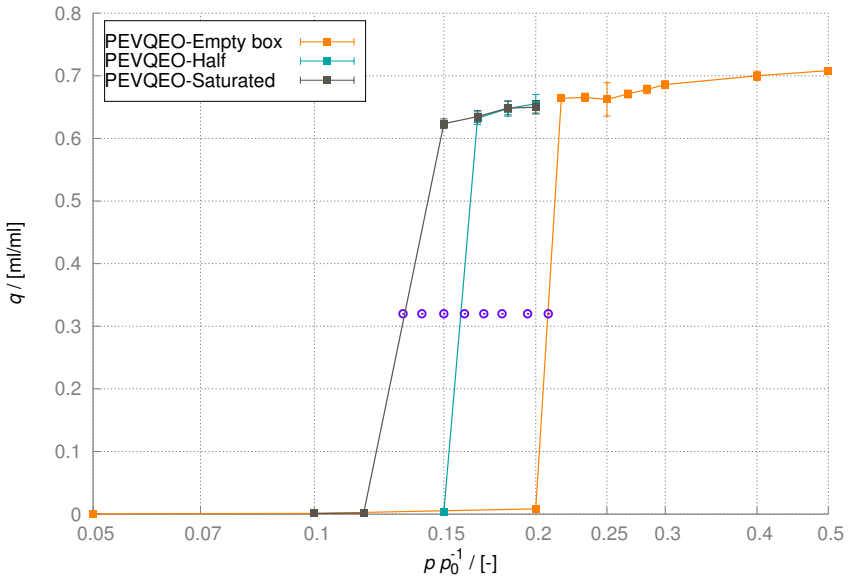

Figure S19: Methanol adsorption isotherms calculated for the PEVQEO structure at 303K. The excess amount of adsorbed methanol as a function of relative pressure ($p\ p_0^{-1}$, where p_0 is the saturation pressure of the adsorbate, $p_0 = 21.7$ kPa).[3] The error bars indicate the 95% confidence intervals.

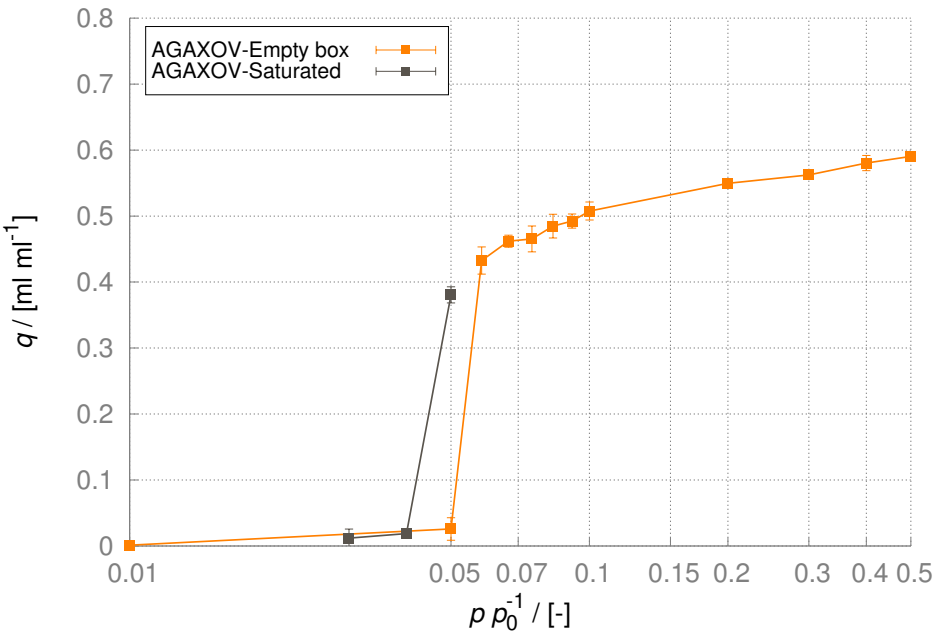

Figure S20: Methanol adsorption isotherms with mid-density method for the AGAXOV structure. The excess amount of adsorbed methanol as a function of relative pressure ($p\ p_0^{-1}$, where p_0 is the saturation pressure of the adsorbate, $p_0 = 21.7$ kPa).[3] The error bars indicate the 95% confidence intervals.

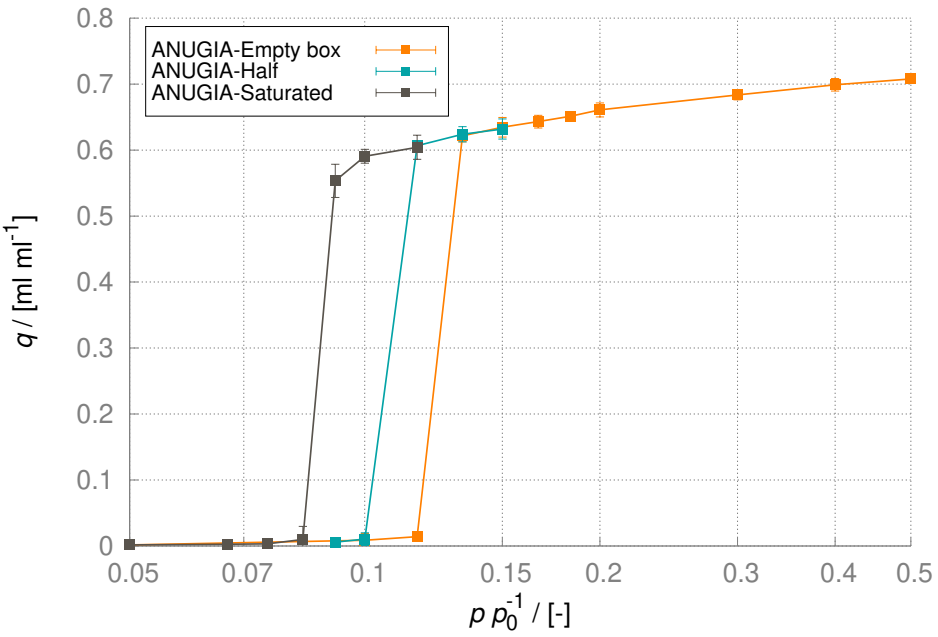

Figure S21: Methanol adsorption isotherms with mid-density method for the ANUGIA structure. The excess amount of adsorbed methanol as a function of relative pressure ($p\,p_0^{-1}$, where p_0 is the saturation pressure of the adsorbate, $p_0 = 21.7$ kPa).[3] The error bars indicate the 95% confidence intervals.

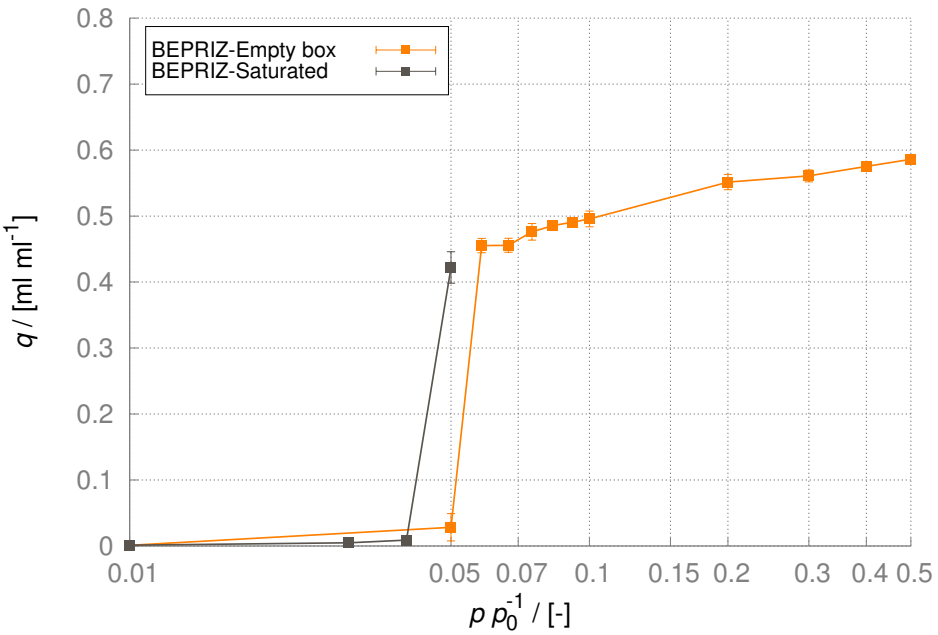

Figure S22: Methanol adsorption isotherms with mid-density method for the BEPRIZ structure. The excess amount of adsorbed methanol as a function of relative pressure ($p\,p_0^{-1}$, where p_0 is the saturation pressure of the adsorbate, $p_0 = 21.7$ kPa).[3] The error bars indicate the 95% confidence intervals.

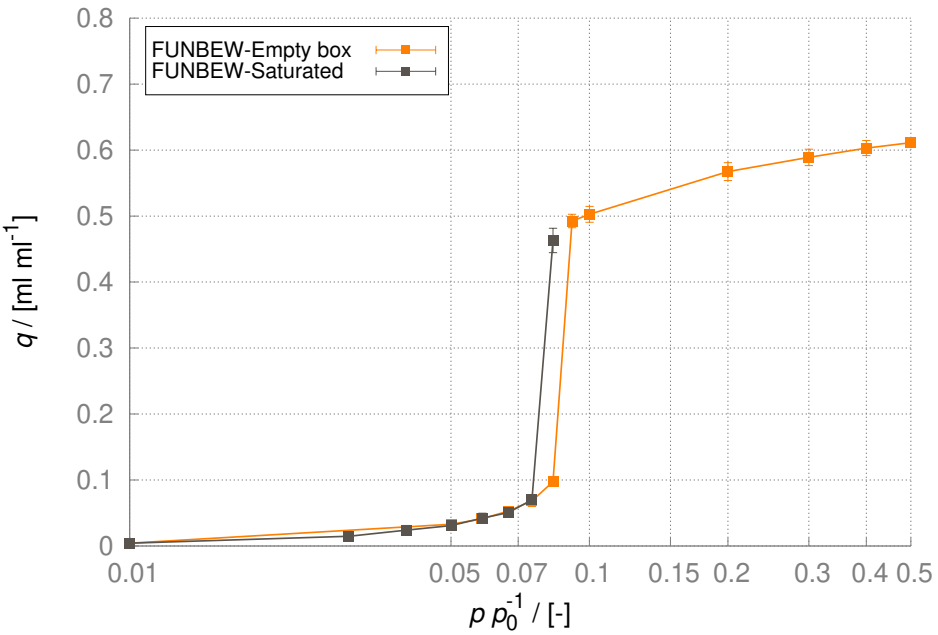

Figure S23: Methanol adsorption isotherms with mid-density method for the FUNBEW structure. The excess amount of adsorbed methanol as a function of relative pressure ($p\ p_0^{-1}$, where p_0 is the saturation pressure of the adsorbate, $p_0 = 21.7$ kPa).[3] The error bars indicate the 95% confidence intervals.

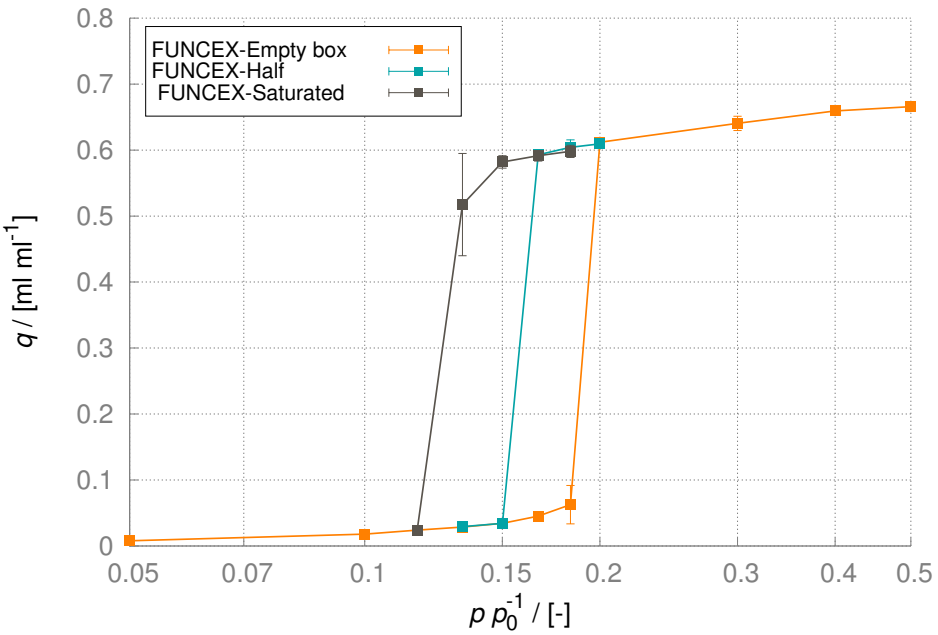

Figure S24: Methanol adsorption isotherms with mid-density method for the FUNCEX structure. The excess amount of adsorbed methanol as a function of relative pressure ($p\ p_0^{-1}$, where p_0 is the saturation pressure of the adsorbate, $p_0 = 21.7$ kPa).[3] The error bars indicate the 95% confidence intervals.

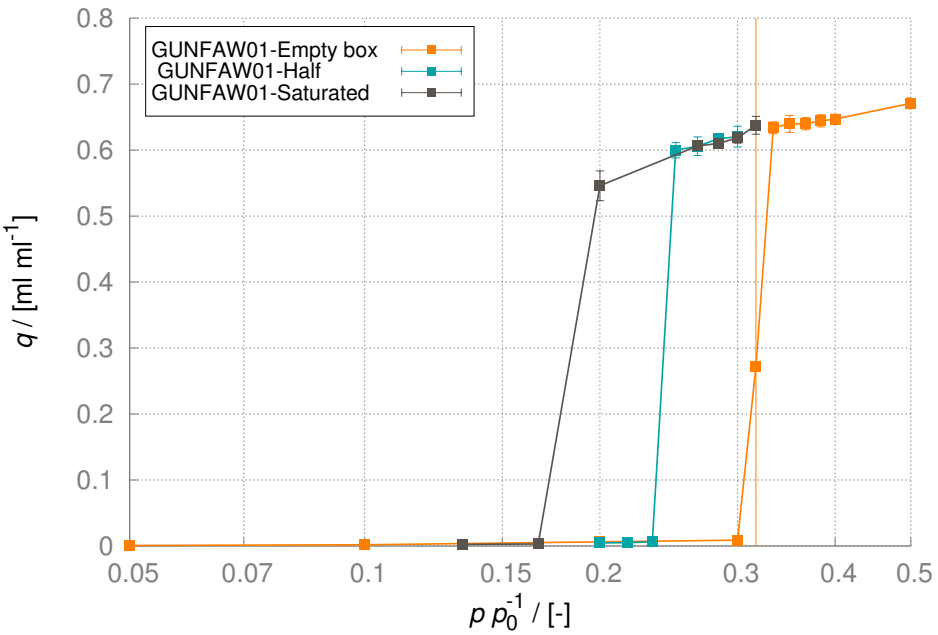

Figure S25: Methanol adsorption isotherm with mid-density method for the GUNFAW01 structure. The excess amount of adsorbed methanol as a function of relative pressure ($p\ p_0^{-1}$, where p_0 is the saturation pressure of the adsorbate, $p_0 = 21.7$ kPa).[3] The error bars indicate the 95% confidence intervals.

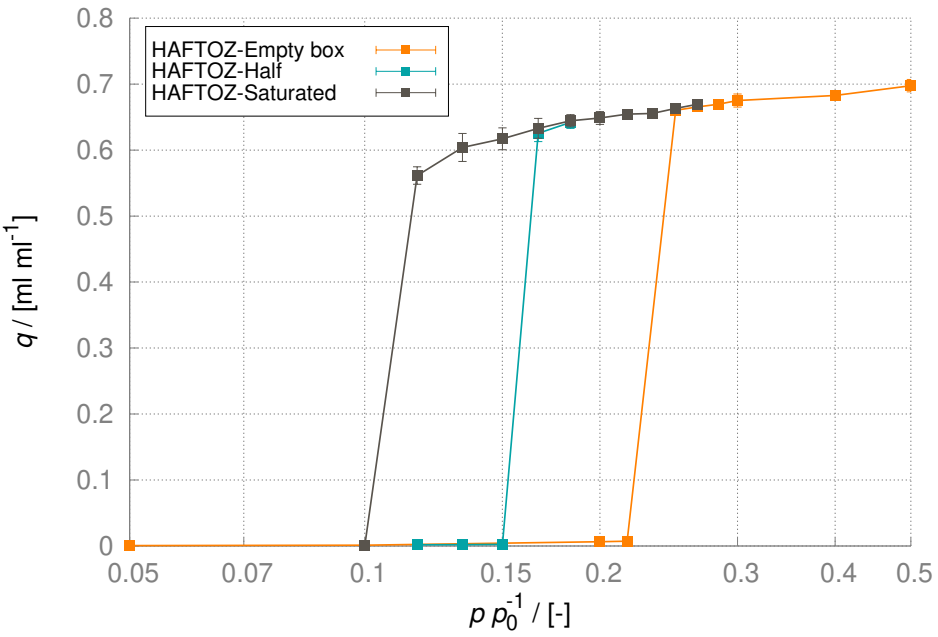

Figure S26: Methanol adsorption isotherm with mid-density method for the HAFTOZ structure. The excess amount of adsorbed methanol as a function of relative pressure ($p\,p_0^{-1}$, where p_0 is the saturation pressure of the adsorbate, $p_0 = 21.7$ kPa).[3] The error bars indicate the 95% confidence intervals.

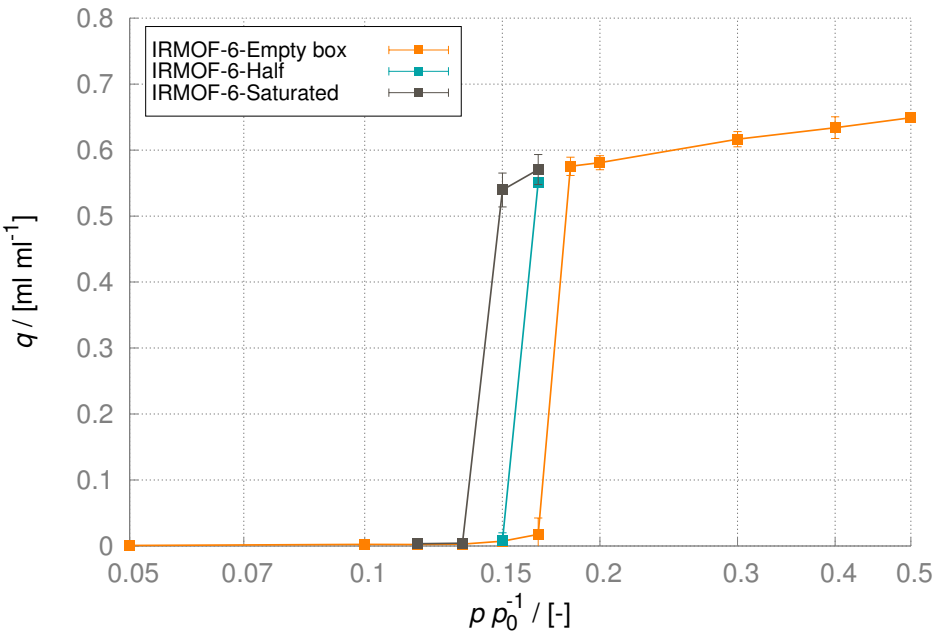

Figure S27: Methanol adsorption isotherm with mid-density method for the IRMOF-6 structure. The excess amount of adsorbed methanol as a function of relative pressure ($p\,p_0^{-1}$, where p_0 is the saturation pressure of the adsorbate, $p_0 = 21.7$ kPa).[3] The error bars indicate the 95% confidence intervals.

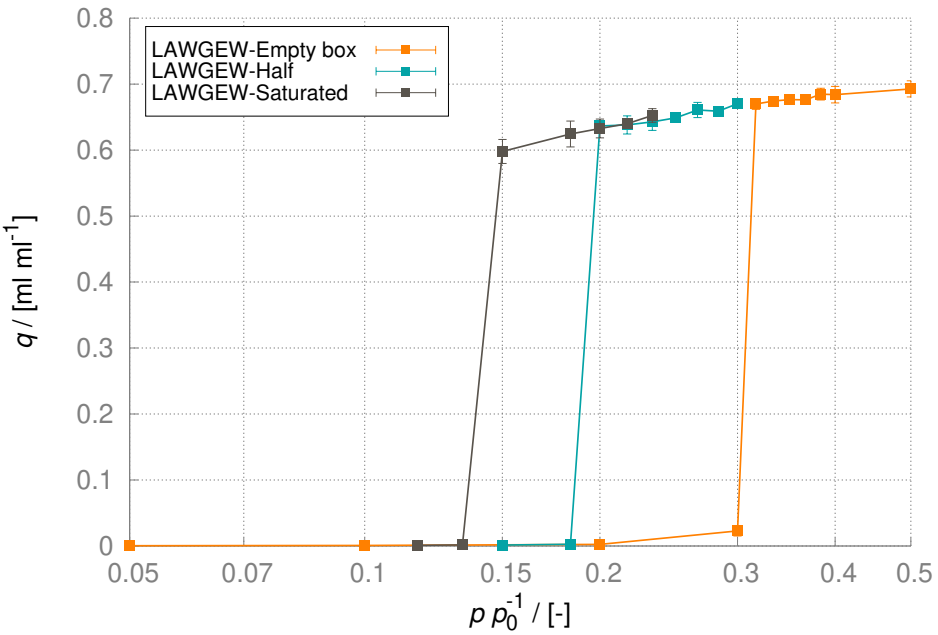

Figure S28: Methanol adsorption isotherm with mid-density method for the LAWGEW structure. The excess amount of adsorbed methanol as a function of relative pressure ($p\ p_0^{-1}$, where p_0 is the saturation pressure of the adsorbate, $p_0 = 21.7$ kPa).[3] The error bars indicate the 95% confidence intervals.

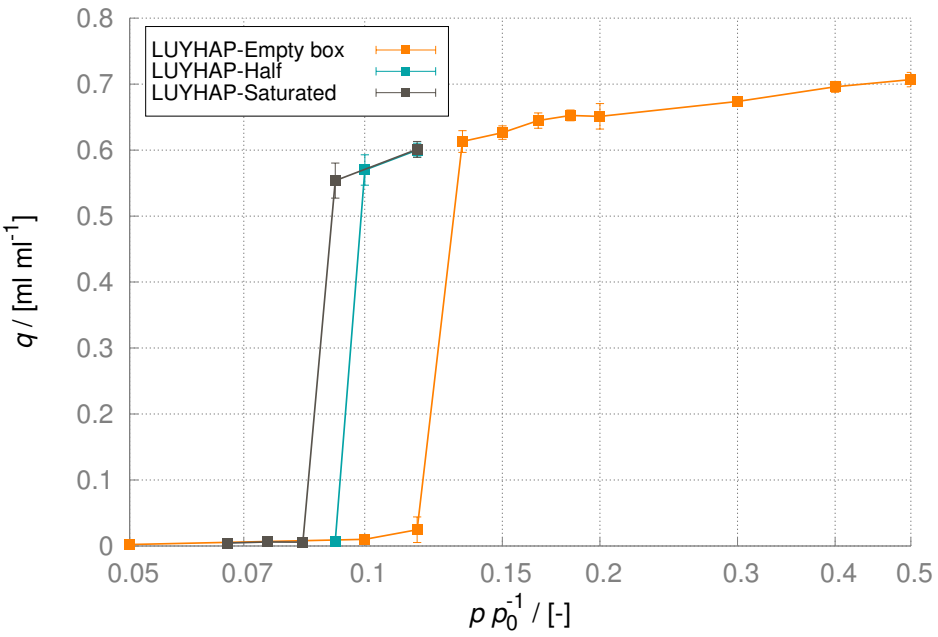

Figure S29: Methanol adsorption isotherm with mid-density method for the LUYHAP structure. The excess amount of adsorbed methanol as a function of relative pressure ($p\,p_0^{-1}$, where p_0 is the saturation pressure of the adsorbate, $p_0 = 21.7$ kPa).[3] The error bars indicate the 95% confidence intervals.

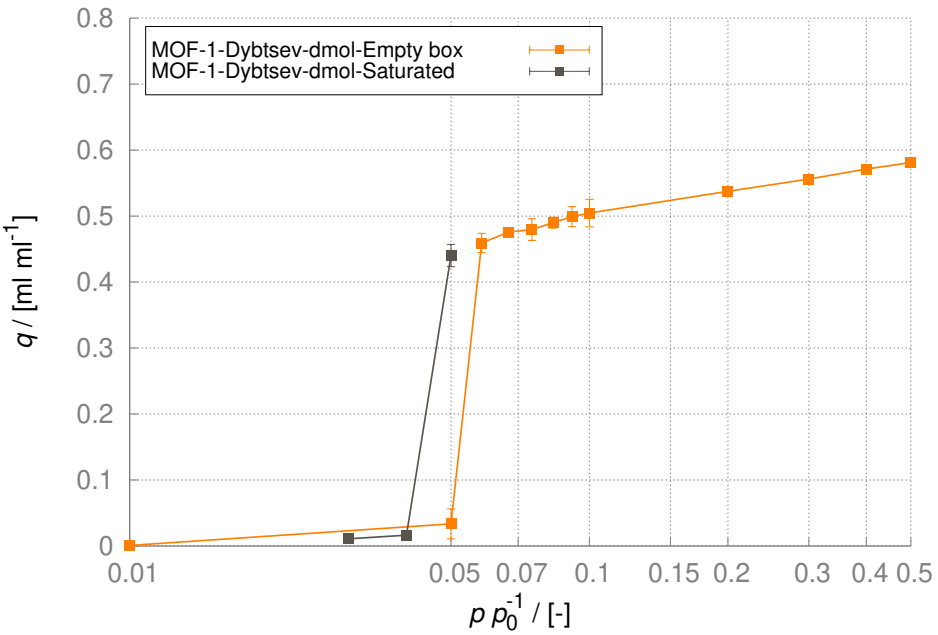

Figure S30: Methanol adsorption isotherm with mid-density method for the MOF-1-Dybtsev-dmol structure. The excess amount of adsorbed methanol as a function of relative pressure ($p\ p_0^{-1}$, where p_0 is the saturation pressure of the adsorbate, $p_0 = 21.7$ kPa).[3] The error bars indicate the 95% confidence intervals.

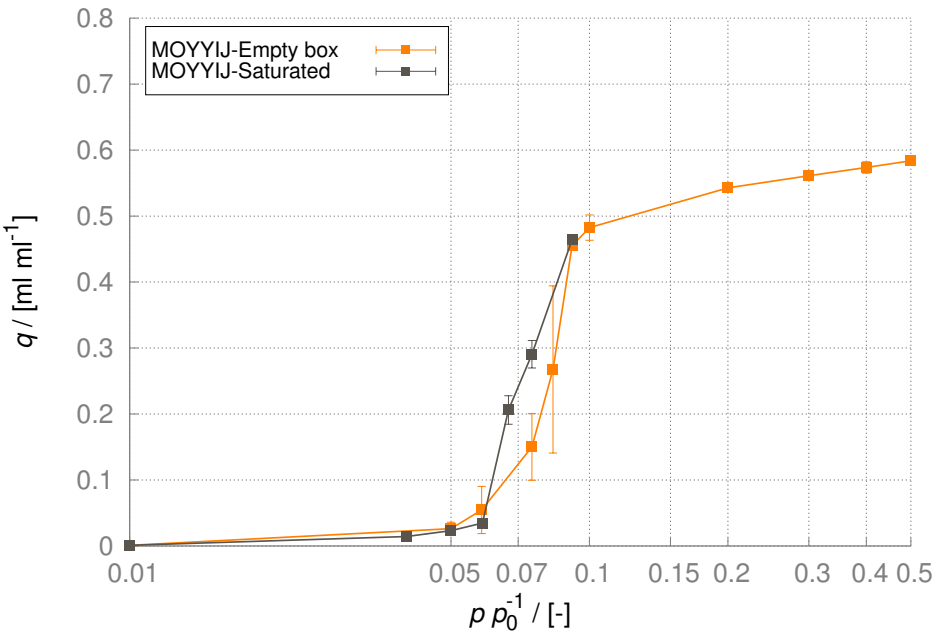

Figure S31: Methanol adsorption isotherm with mid-density method for the MOYYIJ structure. The excess amount of adsorbed methanol as a function of relative pressure ($p\,p_0^{-1}$, where p_0 is the saturation pressure of the adsorbate, $p_0 = 21.7$ kPa).[3] The error bars indicate the 95% confidence intervals.

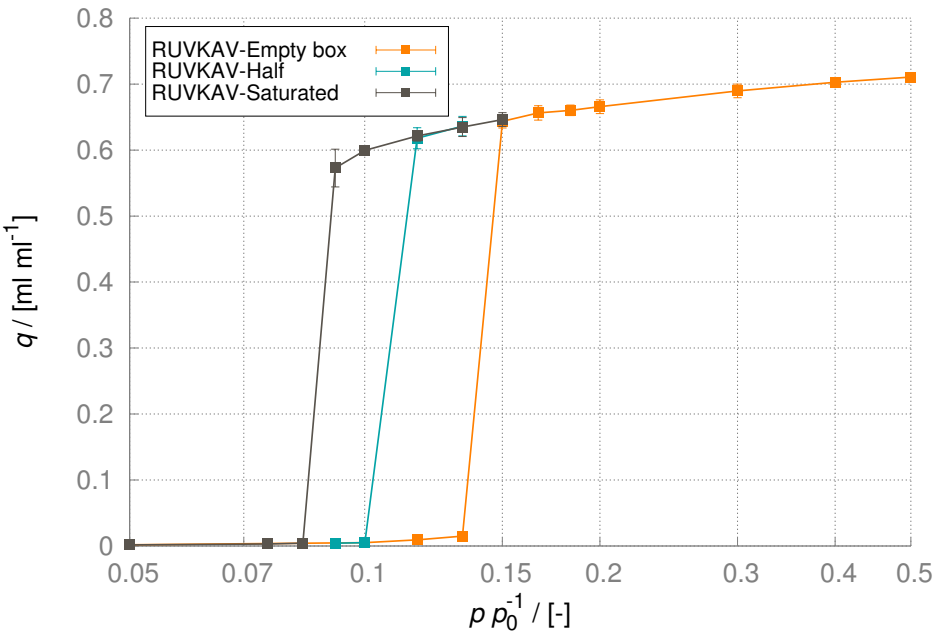

Figure S32: Methanol adsorption isotherm with mid-density method for the RUVKAV structure. The excess amount of adsorbed methanol as a function of relative pressure ($p\,p_0^{-1}$, where p_0 is the saturation pressure of the adsorbate, $p_0 = 21.7$ kPa).[3] The error bars indicate the 95% confidence intervals.

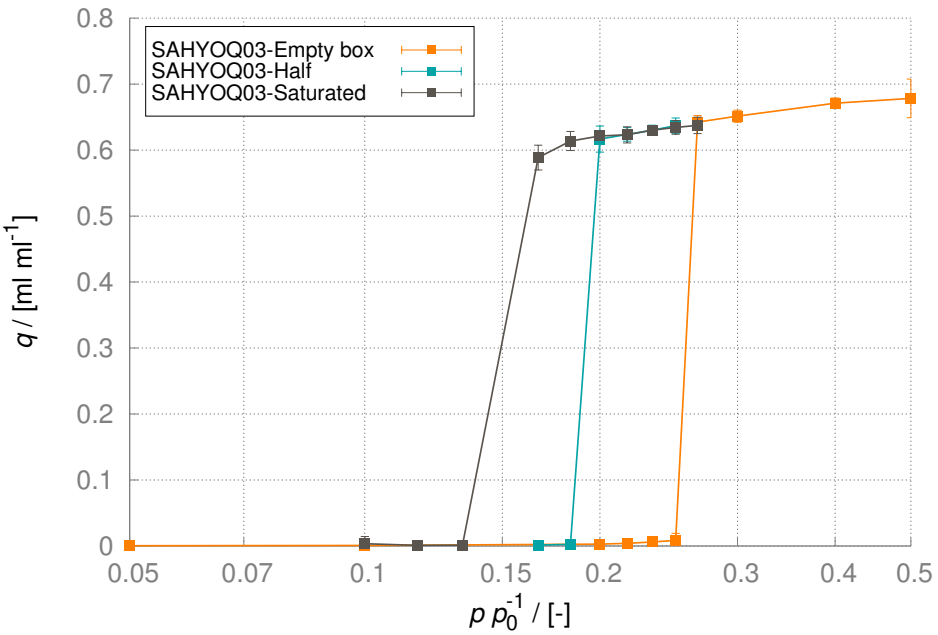

Figure S33: Methanol adsorption isotherm with mid-density method for the SAHYOQ03 structure. The excess amount of adsorbed methanol as a function of relative pressure ($p\ p_0^{-1}$, where p_0 is the saturation pressure of the adsorbate, $p_0 = 21.7$ kPa).[3] The error bars indicate the 95% confidence intervals.

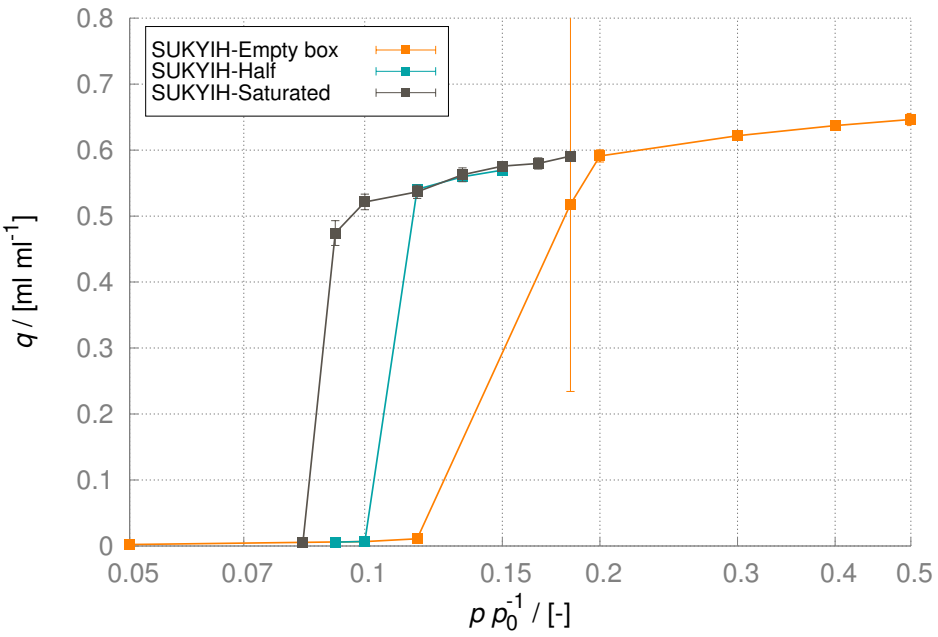

Figure S34: Methanol adsorption isotherm with mid-density method for the SUKYIH structure. The excess amount of adsorbed methanol as a function of relative pressure ($p\,p_0^{-1}$, where p_0 is the saturation pressure of the adsorbate, $p_0 = 21.7$ kPa).[3] The error bars indicate the 95% confidence intervals.

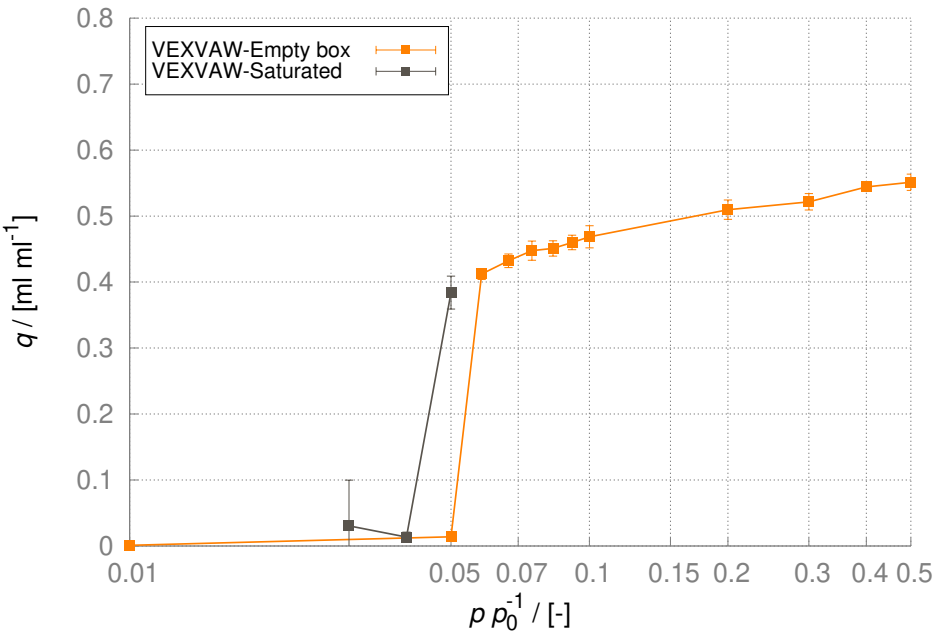

Figure S35: Methanol adsorption isotherm with mid-density method for the VEXVAW structure. The excess amount of adsorbed methanol as a function of relative pressure ($p\,p_0^{-1}$, where p_0 is the saturation pressure of the adsorbate, $p_0 = 21.7$ kPa).[3] The error bars indicate the 95% confidence intervals.

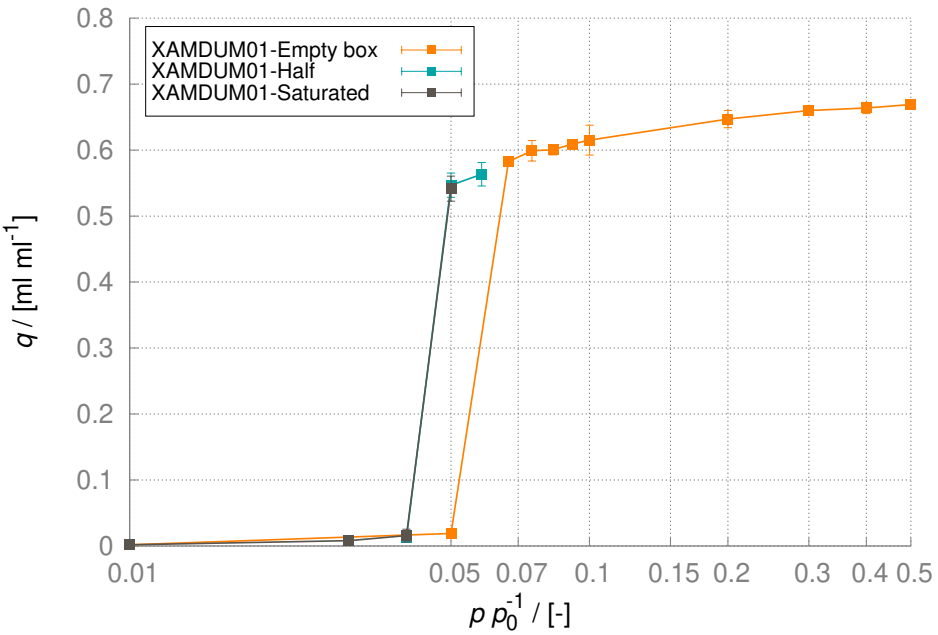

Figure S36: Methanol adsorption isotherm with mid-density method for the XAMDUM01 structure. The excess amount of adsorbed methanol as a function of relative pressure ($p\ p_0^{-1}$, where p_0 is the saturation pressure of the adsorbate, $p_0 = 21.7$ kPa).[3] The error bars indicate the 95% confidence intervals.

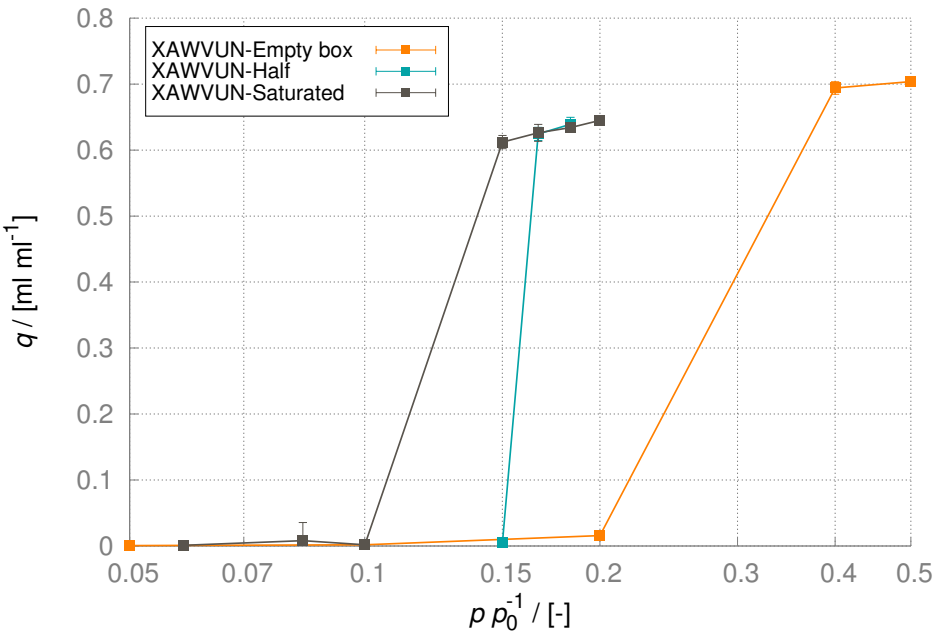

Figure S37: Methanol adsorption isotherm with mid-density method for the XAWVUN structure. The excess amount of adsorbed methanol as a function of relative pressure ($p\ p_0^{-1}$, where p_0 is the saturation pressure of the adsorbate, $p_0 = 21.7$ kPa).[3] The error bars indicate the 95% confidence intervals.

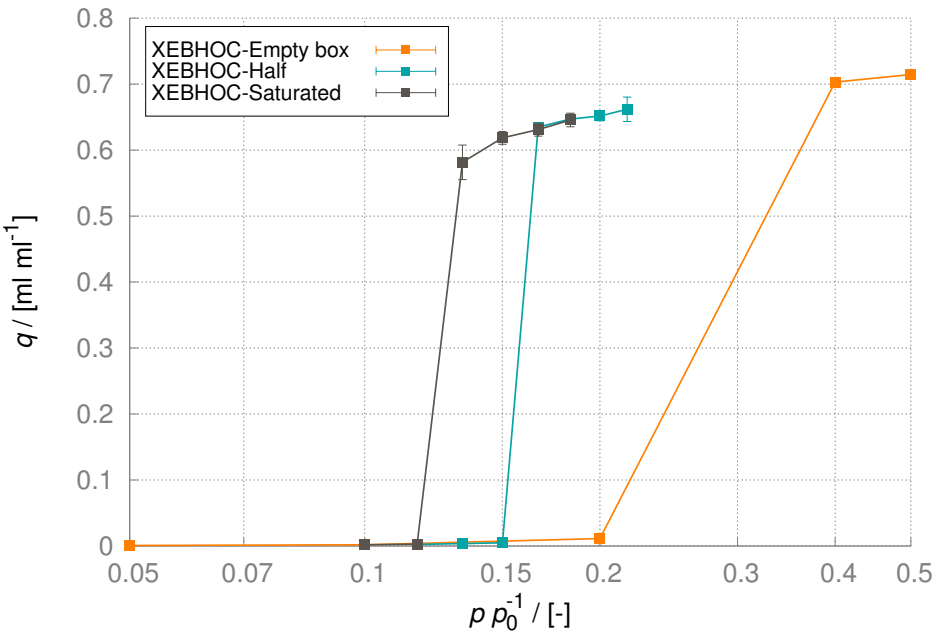

Figure S38: Methanol adsorption isotherm with mid-density method for the XEBHOC structure. The excess amount of adsorbed methanol as a function of relative pressure ($p\,p_0^{-1}$, where p_0 is the saturation pressure of the adsorbate, $p_0 = 21.7$ kPa).[3] The error bars indicate the 95% confidence intervals.

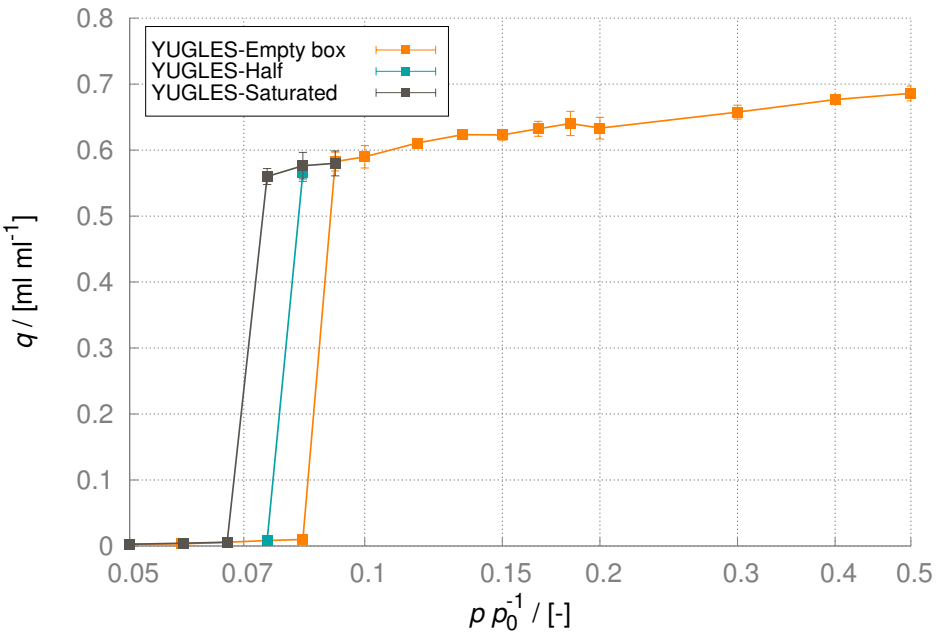

Figure S39: Methanol adsorption isotherm with mid-density method for the YUGLES structure. The excess amount of adsorbed methanol as a function of relative pressure ($p\,p_0^{-1}$, where p_0 is the saturation pressure of the adsorbate, $p_0 = 21.7$ kPa).[3] The error bars indicate the 95% confidence intervals.

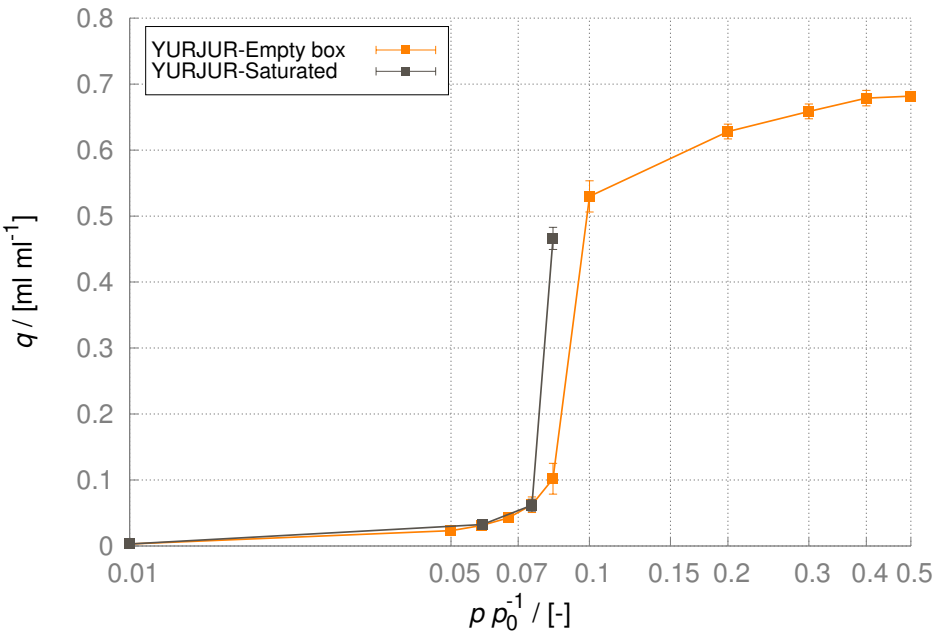

Figure S40: Methanol adsorption isotherm with mid-density method for the YURJUR structure. The excess amount of adsorbed methanol as a function of relative pressure ($p\,p_0^{-1}$, where p_0 is the saturation pressure of the adsorbate, $p_0 = 21.7$ kPa).[3] The error bars indicate the 95% confidence intervals.

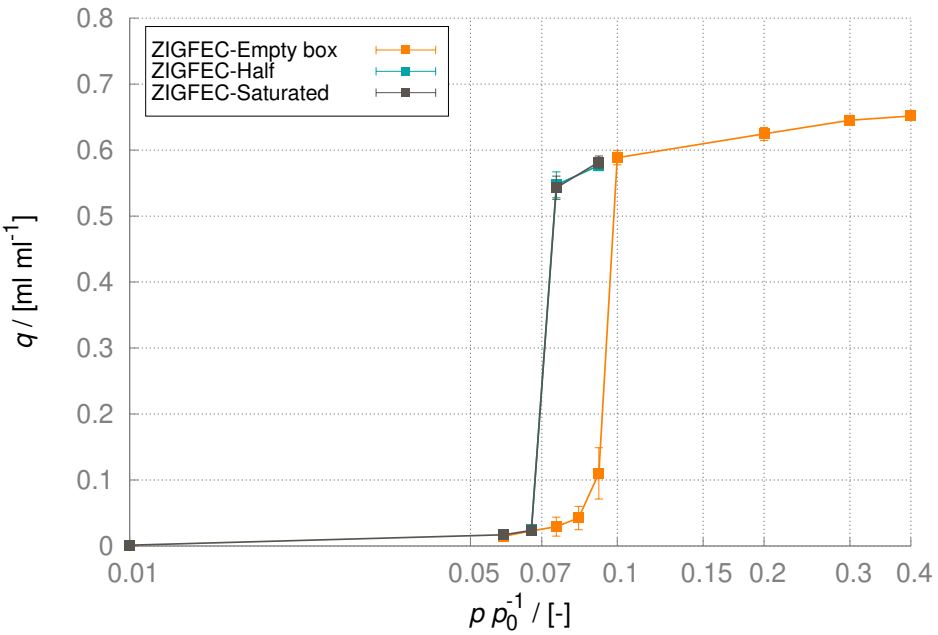

Figure S41: Methanol adsorption isotherm with mid-density method for the ZIGFEC structure. The excess amount of adsorbed methanol as a function of relative pressure ($p\,p_0^{-1}$, where p_0 is the saturation pressure of the adsorbate, $p_0 = 21.7$ kPa).[3] The error bars indicate the 95% confidence intervals.

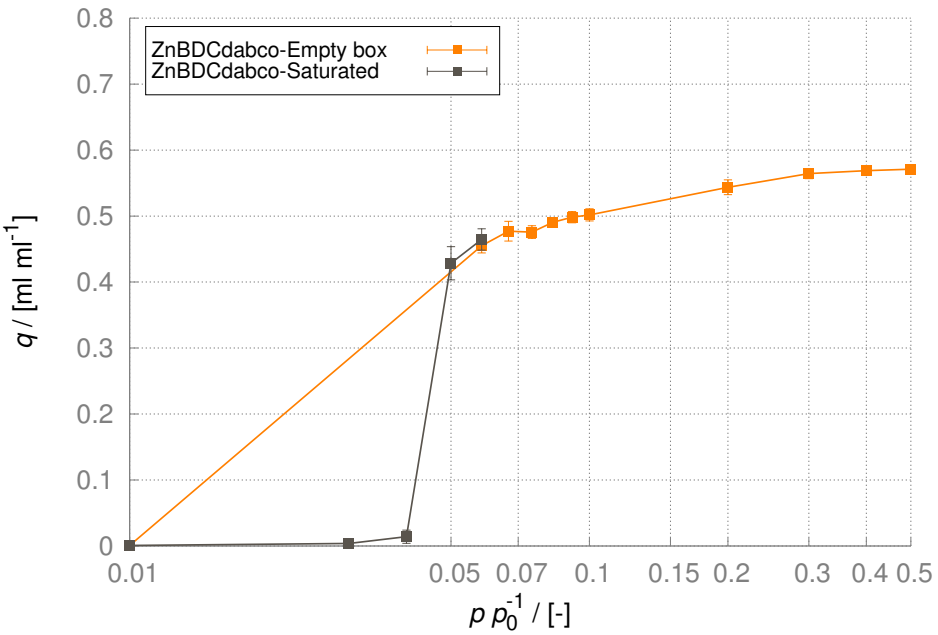

Figure S42: Methanol adsorption isotherm with mid-density method for the ZnBDCdabco structure. The excess amount of adsorbed methanol as a function of relative pressure ($p\ p_0^{-1}$, where p_0 is the saturation pressure of the adsorbate, $p_0 = 21.7$ kPa).[3] The error bars indicate the 95% confidence intervals.

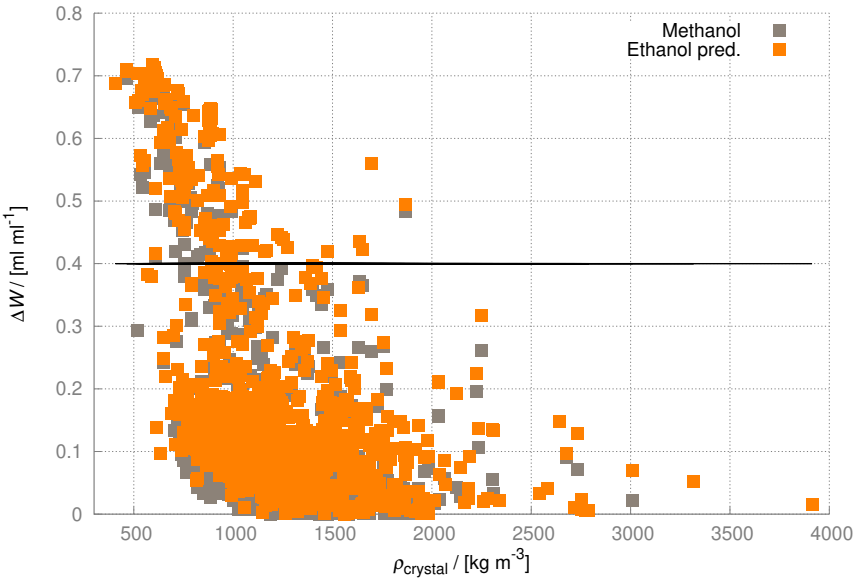

Figure S43: The working capacities of all structures considered in the second screening step with methanol as a function of crystallographic density of the frameworks. The color code represents the calculated methanol (gray), based on the simulation results, and the predicted ethanol working capacities (orange) using Equation 3 in the main text.

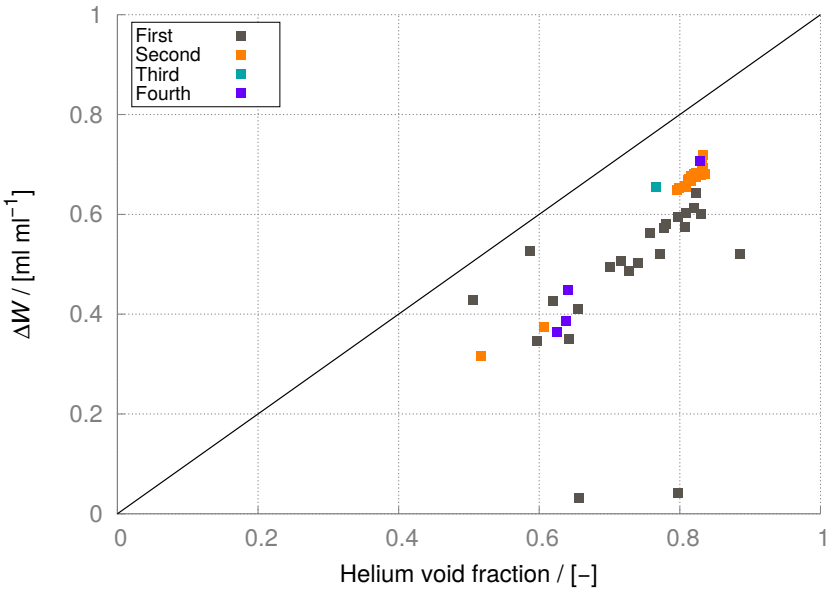

Figure S44: The deliverable working capacity shown as a function of the helium void fraction for the 55 selected structures in the third screening step with ethanol. The color code represents the bin assigned to the given structure. The bins are defined as follows, First: $0.05 \leq \ p\ p_0^{-1} \leq 0.1$, Second: $0.1 < \ p\ p_0^{-1} \leq 0.2$, Third: $0.2 < \ p\ p_0^{-1} \leq 0.3$, Fourth: $0.3 < \ p\ p_0^{-1} \leq 0.4$.

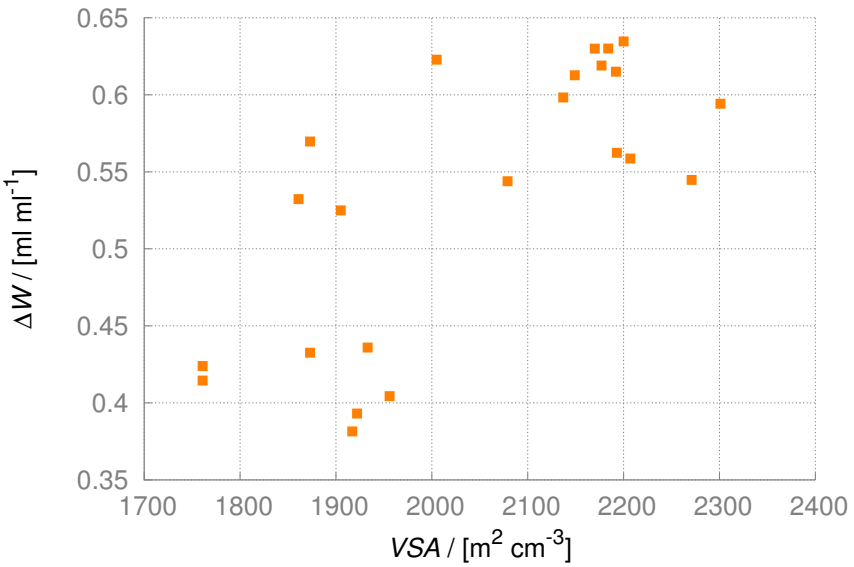

Figure S45: The deliverable working capacity of the best 23 structures with methanol as working fluid as a function of the Volumetric Surface Area (VSA) of each structure.

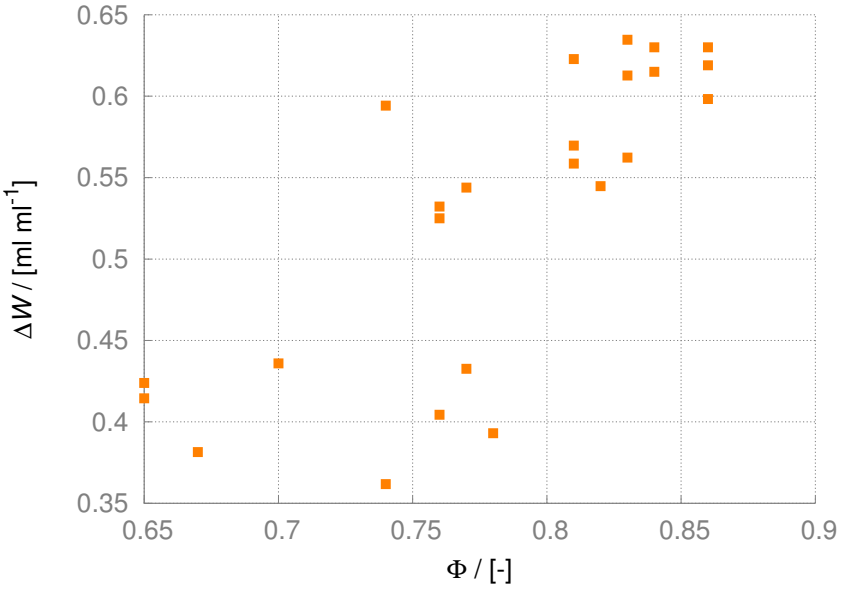

Figure S46: The deliverable working capacity of the best 23 structures with methanol as working fluid as a function of the helium void fraction of each structure.

References

(1) Nazarian, D.; Camp, J. S.; Sholl, D. S. A Comprehensive Set of High-Quality Point Charges for Simulations of Metal–Organic Frameworks. *Chemistry of Materials* **2016**, *28*, 785–793.

(2) Gutiérrez-Sevillano, J. J.; Vicent-Luna, J. M.; Dubbeldam, D.; Calero, S. Molecular Mechanisms for Adsorption in Cu-BTC Metal Organic Framework. *The Journal of Physical Chemistry C* **2013**, *117*, 11357–11366.

(3) Ambrose, D.; Sprake, C. H. S. Thermodynamic properties of organic oxygen compounds XXV. Vapour pressures and normal boiling temperatures of aliphatic alcohols. *The Journal of Chemical Thermodynamics* **1970**, *2*, 631–645.

(4) Comotti, A.; Bracco, S.; Sozzani, P.; Horike, S.; Matsuda, R.; Chen, J.; Takata, M.; Kubota, Y.; Kitagawa, S. Nanochannels of Two Distinct Cross-Sections in a Porous Al-Based Coordination Polymer. *Journal of the American Chemical Society* **2008**, *130*, 13664–13672.

(5) Schneemann, A.; Bon, V.; Schwedler, I.; Senkovska, I.; Kaskel, S.; Fischer, R. A. Flexible metal-organic frameworks. *Chemical Society Reviews* **2014**, *43*, 6062–6096.

(6) Bao, X.; Broadbelt, L. J.; Snurr, R. Q. Computational screening of homochiral metal–organic frameworks for enantioselective adsorption. *Microporous and Mesoporous Materials* **2012**, *157*, 118 – 123.

(7) Wilmer, C. E.; Leaf, M.; Lee, C. Y.; Farha, O. K.; Hauser, B. G.; Hupp, J. T.; Snurr, R. Q. Large-scale screening of hypothetical metal–organic frameworks. *Nature Chemistry* **2012**, *4*, 83–89.

(8) Rappé, A. K.; Casewit, C. J.; Colwell, K. S.; Goddard III, W. A.; Skiff, W. M. UFF, a full periodic table force field for molecular mechanics and molecular dynamics simulations. *Journal of the American Chemical Society* **1992**, *114*, 10024–10035.

(9) Mayo, S. L.; Olafson, B. D.; Goddard III, W. A. DREIDING: a generic force field for molecular simulations. *Journal of Physical Chemistry* **1990**, *94*, 8897–8909.

(10) Eggimann, B. L.; Sunnarborg, A. J.; Stern, H. D.; Bliss, A. P.; Siepmann, J. I. An online parameter and property database for the TraPPE force field. *Molecular Simulation* **2014**, *40*, 101–105.

(11) Schnobrich, J.; Lebel, O.; Cychosz, K.; Dailly, A.; Wong-Foy, A.; Matzger, A. Linker-directed vertex desymmetrization for the production of coordination polymers with high porosity. *Journal of the American Chemical Society* **2010**, *132*, 13941–13948.

(12) Zhao, D.; Yuan, D.; Yakovenko, A.; Zhou, H.-C. A NbO-type metal-organic framework derived from a polyyne-coupled di-isophthalate linker formed in situ. *Chemical Communications* **2010**, *46*, 4196–4198.

(13) Farha, O. K.; Malliakas, C. D.; Kanatzidis, M. G.; Hupp, J. T. Control over catenation in metal-organic frameworks via rational design of the organic building block. *Journal of the American Chemical Society* **2010**, *132*, 950–952.

(14) Lee, C. Y.; Bae, Y.-S.; Jeong, N. C.; Farha, O. K.; Sarjeant, A. A.; Stern, C. L.; Nickias, P.; Snurr, R. Q.; Hupp, J. T.; Nguyen, S. T. Kinetic separation of propene and propane in metal-organic frameworks: Controlling diffusion rates in plate-shaped crystals via tuning of pore apertures and crystallite aspect ratios. *Journal of the American Chemical Society* **2011**, *133*, 5228–5231.

(15) Quartapelle Procopio, E.; Fukushima, T.; Barea, E.; Navarro, J. A. R.; Horike, S.; Kitagawa, S. A soft copper(II) porous coordination polymer with unprecedented aqua bridge and selective adsorption properties. *Chemistry - A European Journal* **2012**, *18*, 13117–13125.

(16) Eddaoudi, M.; Kim, J.; Rosi, N.; Vodak, D.; Wachter, J.; O'Keeffe, M.; Yaghi, O. Systematic design of pore size and functionality in isoreticular MOFs and their application in methane storage. *Science* **2002**, *295*, 469–472.

(17) Sun, D.; Ke, Y.; Mattox, T. M.; Ooro, B. A.; Zhou, H.-C. Temperature-dependent supramolecular stereoisomerism in porous copper coordination networks based on a designed carboxylate ligand. *Chemical Communications* **2005**, 5447–5449.

(18) Dau, P. V.; Kim, M.; Garibay, S. J.; Münch, F. H. L.; Moore, C. E.; Cohen, S. M. Single-atom ligand changes affect breathing in an extended metal-organic framework. *Inorganic Chemistry* **2012**, *51*, 5671–5676.

(19) Quartapelle Procopio, E.; Rojas, S.; Padial, N. M.; Galli, S.; Masciocchi, N.; Linares, F.; Miguel, D.; Oltra, J. E.; Navarro, J. A. R.; Barea, E. Study of the incorporation and release of the non-conventional half-sandwich ruthenium(ii) metallodrug RAPTA-C on a robust MOF. *Chemical Communications* **2011**, *47*, 11751–11753.

(20) Andrés, R.; Brissard, M.; Gruselle, M.; Train, C.; Vaissermann, J.; Malézieux, B.; Jamet, J.-P.; Verdaguer, M. Rational design of three-dimensional (3D) optically active molecule-based magnets. *Inorganic Chemistry* **2001**, *40*, 4633–4640.

(21) Li, K.; Olson, D. H.; Lee, J. Y.; Bi, W.; Wu, K.; Yuen, T.; Xu, Q.; Li, J. Multifunctional microporous MOFs exhibiting gas/hydrocarbon adsorption selectivity, separation capability and three-dimensional magnetic ordering. *Advanced Functional Materials* **2008**, *18*, 2205–2214.

(22) Zhang, K.; Lively, R. P.; Dose, M. E.; Brown, A. J.; Zhang, C.; Chung, J.; Nair, S.; Koros, W. J.; Chance, R. R. Alcohol and water adsorption in zeolitic imidazolate frameworks. *Chemical Communications* **2013**, *49*, 3245–3247.

(23) Van Assche, T. R. C.; Duerinck, T.; Gutiérrez Sevillano, J. J.; Calero, S.; Baron, G. V.; Denayer, J. F. M. High Adsorption Capacities and Two-Step Adsorption of Polar Adsorbates on Copper–Benzene-1,3,5-tricarboxylate Metal–Organic Framework. *The Journal of Physical Chemistry C* **2013**, *117*, 18100–18111.

(24) Fang, Q.-R.; Zhu, G.-S.; Jin, Z.; Xue, M.; Wei, X.; Wang, D.-J.; Qiu, S.-L. A Novel Metal Organic Framework with the Diamondoid Topology Constructed from Pentanuclear Zinc Carboxylate Clusters. *Crystal Growth & Design* **2007**, *7*, 1035–1037.